On the Relative Performance of One-way and Two-way Grid Nesting

Lucas M Harris

A dissertation submitted in partial fulfillment
of the requirements for the degree of

Doctor of Philosophy

University of Washington

2010

Program Authorized to Offer Degree: Department of Atmospheric Sciences

University of Washington
Graduate School

This is to certify that I have examined this copy of a doctoral dissertation by

Lucas M Harris

and have found that it is complete and satisfactory in all respects,
and that any and all revisions required by the final
examining committee have been made.

Chair of the Supervisory Committee:

Dale R. Durran

Reading Committee:

Dale R. Durran

William C. Skamarock

Mark T. Stoelinga

Date:

Signature________________________________

Date____________________________________

University of Washington

Abstract

On the Relative Performance of One-way and Two-way Grid Nesting

Lucas M Harris

Chair of the Supervisory Committee:
Professor and Chair Dale R. Durran
Atmospheric Sciences

Most mesoscale models can be run with either one-way ("parasitic") or two-way ("interactive") grid nesting. This paper presents results from a linear 1D shallow-water model and from 3D simulations of a multicell thunderstorm and of trapped lee waves to determine whether the choice of nesting method can have a significant impact on the solution.

In the shallow-water model, two-way nesting was found to be generally superior to one-way nesting. The increased reflection for longer-wavelength disturbances in the one-way case is due to a phase difference between the coarse- and nested-grid solutions at the nested-grid boundary that accumulates because of the difference in numerical phase speeds between the grids. Reflections for two-way nesting may be estimated from the difference in numerical group velocities between the coarse and nested grids, which only becomes large for waves that are poorly-resolved on the coarse grid. The only situation in which one-way nesting performs better than two-way is when very poorly-resolved waves strike the nest boundary; in these cases, using a filter on the coarse-grid values within the sponge zone of an otherwise conventional sponge boundary condition can greatly reduce the reflections caused by two-way nesting.

The results were more equivocal for the 3D simulations. Two-way nesting clearly produced smaller precipitation errors than did one-way nesting in the multicell simula-

tions, due to the lack of mismatch errors between the coarse- and nested-grid solutions in the two-way simulations. In the trapped lee-wave simulations, two-way nesting produced lower overall errors than did one-way nesting when a simple interpolation BC was used, but larger errors when the sponge BC was used.

TABLE OF CONTENTS

LIST OF FIGURES

Figure Number Page

LIST OF TABLES

ACKNOWLEDGMENTS

I would like to thank my advisor, Dale Durran, for his many contributions to my work during my time here at Washington. I also extend thanks to my committee, Greg Hakim, Bill Skamarock, Mark Stoelinga, and Mitsuhiro Kawase, for their help and suggestions for improving this dissertation. Finally, I must thank my family and many friends for helping me over the past several years as I worked towards my degree.

Chapter 1

INTRODUCTION

Nested grids are extensively used in numerical modeling of the atmosphere for a wide range of applications, including numerical weather prediction (Mass et al., 2002), mesoscale meteorology, regional climate modeling (Giorgi and Mearns, 1999), and air quality modeling (Krol et al., 2005). A model which uses grid nesting must specify how the grids communicate with one another, which has two separate parts. All nested grid models will use the coarse grid data to specify the boundary conditions (BCs) of the nested grid; if this is the only communication between the grids, the model is said to use one-way (parasitic) nesting since information is only transferred from the coarse to the nested grid. Many models will also use the nested grid solution to correct that on the coarse grid in what is called two-way (interactive) nesting, since information is also transferred from the nested to the coarse grid.

This dissertation will address the differences between one-way and two-way nesting in both highly idealized and more realistic contexts. The goal will be to determine which nesting strategy is superior in a number of situations, and why. Chapter 2, taken from Harris and Durran (2010, accepted to MWR), analyzes differences between the nesting strategies in a one-dimensional shallow-water model whose behavior can be analyzed without undue complication. The analysis will examine reflections of a localized disturbance exiting the nested grid using either of two common nested grid BCs: simple interpolation and a Davies (1976) sponge layer. Although the interpolation BC is not particularly effective at eliminating reflections, we consider it because it allows for a simple analytic expression for the amplitude of reflections at the nested-grid boundary using either nesting strategy, and allows us to build a theory useful for analyzing the more complicated cases discussed in the rest of the thesis.

Chapter 3 presents simulations of complex meteorological flows which demonstrate sensitivity to the nesting methodology. We do not aim to give a comprehensive description of how the dynamics are altered in the presence of the nest's boundaries, but instead to show sensitivity to the nesting strategy in realistic simulations of mesoscale phenomena. First examined are quasi-two-dimensional simulations of trapped waves in the lee of a mountain ridge. Numerical models are known (Reinecke and Durran, 2009) to inaccurately simulate topographic waves resolved by as many as 8 grid points, resulting in errors in the direction of propagation and in horizontal group velocity. Open BCs are known to produce substantial reflections of trapped lee waves, and nested grid BCs are expected to have similar difficulties.

Also described in Chapter 3 are errors introduced by grid nesting in a fully three-dimensional simulation of a multicell thunderstorm. Organized convection is known to be sensitive to computational resolution (Weisman et al., 1997) as more poorly-resolved convective cells will evolve and propagate more slowly. The change in grid spacing between the nested and coarse grids is thus expected to be difficult for a storm attempting to exit the nested grid. Simulations of both phenomena will be studied for errors with clear meteorological significance: reflected trapped waves in the lee wave simulations, and precipitation errors in the multicell simulations.

Some modelers may be concerned that the use of two-way nesting could distort the coarse-mesh solution and make it less cosmetically appealing. Chapter 4 will briefly address the impact of two-way nesting on the coarse-grid solution using a simple advection problem and whether the distortion results in a less accurate solution. A synthesis of results will be presented in the concluding Chapter 5.

1.1 Background and review

The implementation and proper use of grid nesting requires attention to intergrid communication, which can be split into two different problems. The first part is communication from the coarse grid to the nested grid, typically through the specification of the boundary conditions of the nested grid. The conditions at the nested grid boundary must satisfy the radiation condition that outgoing disturbances should leave the nested grid without causing reflections back into the domain, but also allow disturbances on the coarse grid to propagate onto the nested grid without distortion. Several such BCs are reviewed in Zhang et al. (1986) and Staniforth (1997).

The second part of the grid communication problem is that from the nested to the coarse grid, also referred to as coarse-grid updating. Many mesoscale models give the choice of either one-way nesting or two-way nesting. One-way nesting performs no nested-to-coarse grid communication; the solution on the coarse grid is simply independent of that on the nested grid. On the other hand, in two-way nesting the solution on the coarse grid is continually replaced (or "updated") by that on the nested grid wherever the two grids coincide. A number of update algorithms have been proposed; see Zhang et al. (1986) and Skamarock and Klemp (1993) for some examples.

Admonitions to use two-way nesting are occasionally seen in the literature (Warner et al., 1997; Clark and Farley, 1984; Phillips and Shukla, 1973), but the few examples given supporting this assertion do not show a dramatic difference between one- and two-way nesting, and one-way nesting is still used in some applications (Mass et al., 2002; Colle et al., 2005; Deng and Stull, 2005) and in some operational forecasts (Table 1).

Warner et al. (1997) recommend using two-way nesting whenever possible since the solution is presumed to be more accurate when the coarse and nested grid solutions are allowed to interact with one another. However, they note that the potential

Organization	Model	Resolutions	Method
Washington	WRF	36, 12, and 4 km	One-way
Wisconsin	UW-NMS	160, 80, and 27 km	Two-way
Oklahoma	ARPS/wx	27, 9, and 3 km	One-way
NCAR AMPS	WRF	45, 15, 5, and 1.7 km	Both
NCAR Real-time	WRF	36 and 12 km	Two-way
Penn State	WRF	36, 12, 4, 1.33 and 0.44 km	One-way
NRL	COAMPS-OS	27, 9, 3, and 1 km*	One-way
Colorado State	RAMS**	48, 12, and 3 km	Two-way
FSL	RUC-HRRR	13 and 3 km	One-way

Table 1.1: Selected forecast mesoscale models and their nesting methodology. *For the Washington, D.C. forecast area; Gulf of Mexico and San Francisco forecast areas use slightly different nesting methodologies and lower resolutions, but still use one-way nesting. Recent real-time hurricane simulations with COAMPS-OS use two-way nesting. **RAMS no longer operational at the time of writing.

improvements of two-way nesting have not been confirmed by research.

Elsberry (1978) discusses potential problems with one-way nesting. In particular, he notes that the phase speed and amplitude of a solution which is poorly-resolved on the coarse grid but well-resolved on the nested grid will differ, so that disturbances which are represented on both grids will reach the nested-grid boundary at different times. This would cause a mismatch at the boundary of the nested grid and thus cause spurious reflections to contaminate the nested-grid solution. This problem would not be present at the boundary of a two-way nested grid, and therefore Elsberry expects the errors to be reduced in a two-way nested simulation. However, he does not test these problems with numerical experiments and does not perform any quantitative analysis of what errors might be expected.

Sundstrom and Elvius (1979) claim that two-way nesting may give *larger* errors than one-way nesting due to reflections caused by the change of group velocities between the nested and coarse grids. However, they also do not give any examples supporting this assertion, and furthermore do not consider similar effects when using one-way nesting.

Harrison and Elsberry (1972) compared a single one-way simulation (called "independent coarse-mesh grid") of the one-dimensional scalar advection equation to compare with a two-way simulation ("mutually determined"). Nested grid BCs were specified by interpolating from the coarse to a single point at each end of the nested grid; we will refer to this technique, very common in nested grid modeling, as the "interpolation BC". A two-way nested grid caused little change to the solution as it propagated across the nested-grid boundary, but substantial noise appeared at the boundary of the one-way nest. No explanation was given for the poor performance of the one-way simulation.

Phillips and Shukla (1973) studied the distortion of shallow-water Rossby and gravity waves in simulations using both a one-way and a two-way nest. They solved the two-dimensional nonlinear shallow-water equations in a uniform westerly mean flow on an f-plane discretized using the Lax-Wendroff scheme on a grid staggered in both time and space. Nested-grid solutions (using the interpolation BC) were compared against a control simulation consisting of a single doubly-periodic grid covering the coarse-grid domain and having the same resolution as the nested grid.

It was found that the solutions for a two-way nest were "almost invariably nearer" to the corresponding control case. This can be seen in Fig. 1.1 for two simulations of monochromatic gravity waves, each propagating in a different direction against the mean westerlies. While the nested-grid simulations deviate significantly from the control simulation for both tests, the two-way simulations lack the noise near the boundaries characteristic of the one-way simulations. Similar results were found in other tests; in particular, a simulation of a Rossby wave found that using two-way nesting could reduce the error in the geopotential field by nearly twenty percent compared to one-way nesting. The authors claimed that the two-way solution is more accurate than the one-way solution because coarse-grid solution is nearer to that on the nested grid, but they do not elaborate on this rather obvious point. In particular there is no analysis of why reflections might be lower when using two-way nesting.

Clark and Farley (1984) and Chen (1991) both performed simulations of two-dimensional linear, vertically-propagating mountain waves using nested grids to increase both the horizontal and vertical resolution near the mountain. Clark and Farley (1984) found that their anelastic simulations clearly produced a solution with less reflection off of the top boundary when two-way nesting was used instead of one-way nesting (Fig. 1.2). However, their model used "vertical nesting" in which the nested grid's upper boundary did not coincide with the coarse grid's upper boundary. This method is not used in most mesoscale models; see Mahalov and Moustaoui (2009) for a recent discussion of this topic. Clark and Farley (1984) did not use the interpolation BC, but instead linearly interpolated *fluxes* to the boundary of the nested grid. This approach yields conservation of mass and momentum across the nested-grid boundary, which is a desirable property for some modelers (Kurihara et al., 1979; Peng et al.,

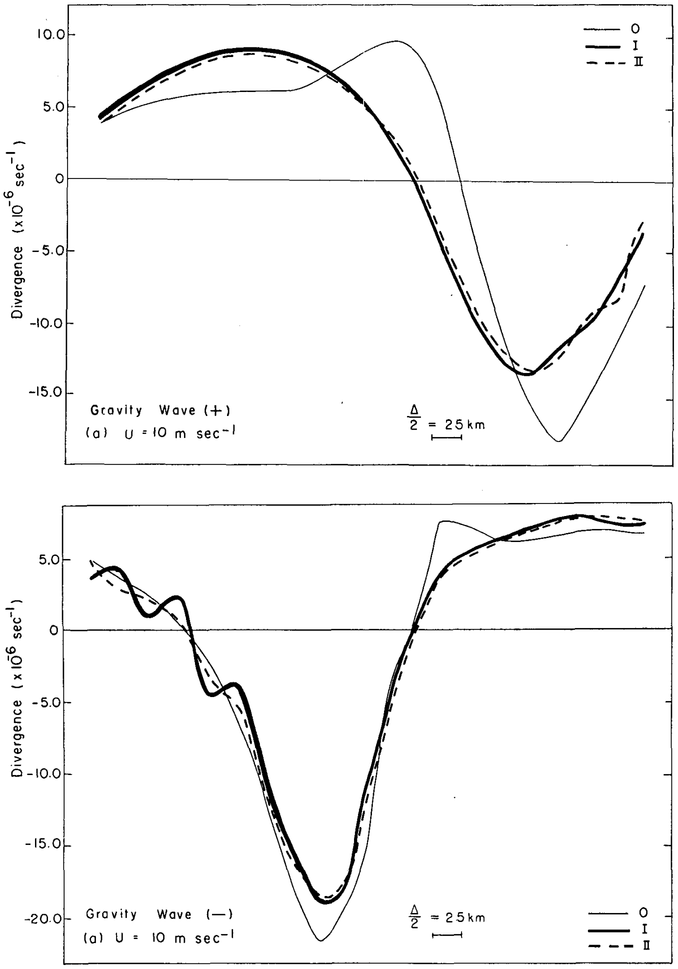

Figure 1.1: Nested-grid horizontal divergence from nonlinear shallow-water simulations of a gravity wave from Phillips and Shukla (1973). Results are shown at $t = 12$ hr along the east-west centerline of the nested grid. Thin solid line denotes the control simulation ("0"); heavy solid line denotes a one-way nested simulation ("I"); heavy dashed line denotes two-way nested simulation ("II"). (Top) Eastward- (rightward-) propagating wave; (bottom) westward- (leftward-) propagating wave. The distance between gridpoints on the nested grid is indicated by measurement bar in lower portion of each figure. (©1973 American Meteorological Society. Used with permission.)

2006) but lies beyond the scope of our research.

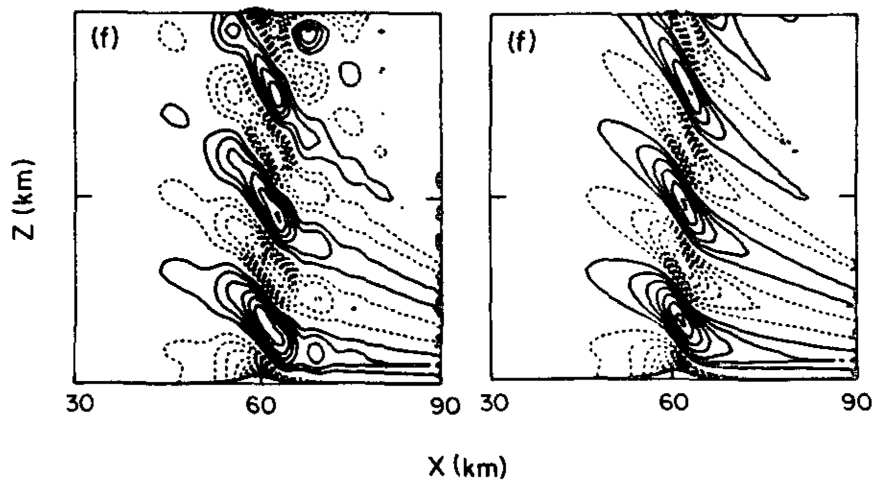

Figure 1.2: Streamline displacement on the nested grid in two-dimensional simulations of anelastic flow over an isolated ridge from Clark and Farley (1984), negative contours dashed. Left: one-way simulation; right: two-way simulation. (©1984 American Meteorological Society. Used with permission.)

(Chen, 1991) used a similar nesting strategy in a fully compressible model to test several different boundary conditions, including the interpolation BC and a continuously-stratified variant of the inflow-outflow BC of Carpenter (1982) for shallow water flow. To avoid having the model's timestep restricted to that required for stability of sound waves (absent in the anelastic simulations of Clark and Farley (1984)) Chen used the partial time-splitting technique of Klemp and Wilhelmson (1978) allowing the acoustic terms in the governing equations to be computed on a smaller "acoustic" timestep than those relevant for gravity wave propagation. Using this technique was however found to greatly increase reflections of sound waves when using the interpolation BC in two-way nesting (Fig. 1.3a). This was attributed to the fact that, while the BCs are not held fixed over each acoustic timestep, the two-updating process is not performed each acoustic timestep. The coarse grid's data, imposed through the interpolation BC, becomes increasingly incompatible with the nested grid solution during the acoustic timesteps, and the advantages of two-way nesting are lost. The resulting mismatch creates sound waves which are eventually updated to the coarse grid, which can feed back through the BCs onto the nested grid and steadily amplify. A two-way simulation without time-splitting (Fig. 1.3b) did not create such noise, and produced a superior solution to the one-way nested simulation with time splitting and the interpolation BC (Fig. 1.3c). Applying the Carpenter BC improved both the one-way and two-way nested solutions, in which the latter produced no sound-wave reflections. Chen did not present any results using one-way nesting without time splitting.

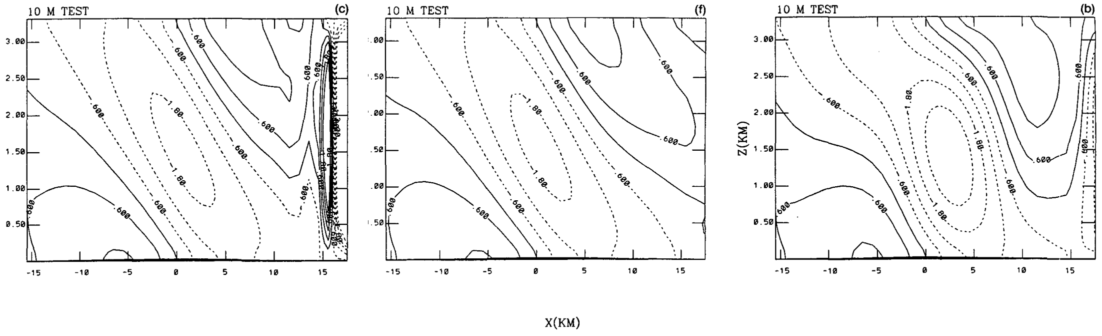

Figure 1.3: Vertical velocity on the most-deeply-nested grid in two-dimensional simulations of fully-compressible flow over an isolated ridge from Chen (1991), negative contours dashed. Left: two-way simulation with time splitting; center: two-way simulation without time splitting; right: one-way simulation with time splitting. (©1991 American Meteorological Society. Used with permission.)

Other researchers have not had the same problem using two-way nesting in a fully-compressible time-split model. Skamarock and Klemp (1993) used dynamically-created nested grids with the interpolation BC to locally increase the resolution of a simulated supercell thunderstorm. No significant errors caused by reflections of sound waves were observed, which was attributed to the use of a reduced sound speed at the nested-grid boundary during the small timestep computations, the use of divergence damping to filter sound waves, and the use of moving grids which limited the amount of interaction poorly-resolved features had with the nested-grid boundaries.

Some authors have attempted to derive analytic formulas for the amplitudes of the reflections or for other errors caused by the use of different grid-nesting techniques and BCs. Vichnevetsky (1981) analyzed the reflections in the one-dimensional scalar advection equation that occur as a wave propagates through a grid refinement, which is similar to a wave propagating out of a two-way nested grid. He found that the reflection coefficient, or the ratio of the amplitudes of the incident and reflected waves, can be determined through a simple expression involving the discrete group velocities on either side of the refinement, an effect predicted by Sundstrom and Elvius (1979). Mar-Or and Givoli (2006) carefully analyzed reflections in the 1D linear shallow-water equations using the Carpenter (1982) BC at the edge of a one-way nest, but they did not consider two-way nests or a wider range of practically important boundary conditions.

Very recently, Schroeder and Schlünzen (2009) examined reflections of Boussinesq gravity waves from the boundary of a two-way nest for a number of different refinement ratios—the ratio of grid spacing on the coarse grid to that on the nested grid—for disturbances of different horizontal resolutions. They found that reflections from the interpolation BC became increasingly severe for higher refinement ratios, since solutions which are well-resolved on the nested grid become increasingly poorly-resolved on the coarse grid as the refinement ratio increases. Similar to the analysis of Vichnevetsky, they found that the amplitude of the reflected disturbance was dependent upon the difference in numerical group velocities between the two grids; since the group velocity error is larger for more poorly-resolved solutions (a result also found for Boussinesq gravity waves by Reinecke and Durran, 2009), larger refinement ratios are expected to yield larger reflections. Schroeder and Schlünzen (2009) recommend using refinement ratios no larger than three to avoid producing unacceptably large reflections. They do not examine the effect of different refinement ratios on reflections caused by one-way nesting, nor do they attempt to compare their numerical results to an analytical estimate of the reflection amplitudes.

Chapter 2

IDEALIZED SIMULATIONS WITH A ONE-DIMENSIONAL SHALLOW-WATER MODEL

In this chapter we explore the sensitivity to one-way and two-way nesting in a simple shallow-water model. The reflections of localized wave packets of a range of resolutions will be tested in both nesting strategies and for both the interpolation and sponge BCs. These results will then be compared to theoretical estimates for the reflections when using the interpolation BC. Two-way nesting will cause much smaller reflections than one-way nesting for all but the most poorly-resolved wavelengths, since two-way nesting avoids the accumulation of phase errors between the coarse and nested grids that leads to a mismatch and reflection at the nested grid boundary.

2.1 Model Description and Methodology

The one-dimensional linear shallow-water model is described by the equations:

$$\frac{\partial u}{\partial t} + g\frac{\partial h}{\partial x} = 0 \tag{2.1}$$

$$\frac{\partial h}{\partial t} + H\frac{\partial u}{\partial x} = 0 \tag{2.2}$$

for velocity u, perturbation interface height h, gravitational acceleration $g = 9.8$ m s^{-2}, and mean water depth H, which is chosen to satisfy $\sqrt{gH} = c = 5$ m s^{-1}, where c is the shallow-water wave speed. There is no mean flow, Coriolis, or topography in these experiments.

The equations are discretized on a staggered Arakawa C-grid, using second-order centered differencing in space and leapfrog differencing in time:

$$\begin{aligned} \delta_{2t}u + g\delta_x h &= 0 \\ \delta_{2t}h + H\delta_x u &= 0. \end{aligned}$$

The finite difference operators above are defined by the expression

$$\delta_{nx}\phi(x) = \frac{\phi(x + n\Delta x/2) - \phi(x - n\Delta x/2)}{n\Delta x} \tag{2.3}$$

for x, and similarly for t.

The simulations in this paper all use a periodic coarse grid with a x-direction width L_{xc} of 16 km and a nested grid whose western boundary is at 5 km and whose width is $L_{xn} = 6$ km, unless otherwise specified. On the coarse grid, $\Delta x_c = 20$ m, and $\Delta t_c = 0.4$ s, giving a Courant number of $c\Delta t/\Delta x = 0.1$. Grid nesting is implemented with a 3:1 refinement in space and time, as in many widely-used mesoscale models, giving a nested-grid spacing of $\Delta x_n = 6.7$ m and timestep of $\Delta t_n = 0.13$ s. Numerical simulations with the Courant number halved to 0.05 give almost the same results (to within 4%), as do simulations integrated using the third-order Adams-Bashforth method (Durran, 1991) with $c\Delta t/\Delta x = 0.1$. Thus, our simulations may be interpreted as isolating the effects of the spatial discretization on the solution.

Two types of nested-grid BC are used. The first, called the "interpolation" BC, merely interpolates the coarse-grid data to the boundary points on the nested grid for all variables on each nested grid timestep. This is the simplest "open" boundary condition for nested grids allowing both outflow and inflow, and allows for comparatively simple analytic expressions for the reflection amplitude. However, this BC performs substantially worse than other nested-grid BCs used in recent mesoscale models. The second BC uses the sponge-layer formulation in the Weather Research and Forecasting (WRF) model's Advanced Research WRF dynamical core (Skamarock et al., 2005) for nested grids as of version 2.1.1 (as quoted in Moeng et al., 2007), in which the outermost point of the nested grid is interpolated, and the solution for each variable on the next N points in from the boundary (collectively, the "sponge zone") are given as:

$$\begin{aligned} \left.\frac{\partial u}{\partial t}\right|_n &= -g\frac{\partial h}{\partial x} + w_{1n}\left(u_c - u_n\right) - w_{2n}\Delta^2\left(u_c - u_n\right) \\ \left.\frac{\partial h}{\partial t}\right|_n &= -H\frac{\partial u}{\partial x} + w_{1n}\left(h_c - h_n\right) - w_{2n}\Delta^2\left(h_c - h_n\right) \end{aligned} \tag{2.4}$$

where n is the index of this grid point in the sponge zone (counting inward from the interpolated point), u_c represents data interpolated from the coarse grid to the same point as u_n, Δ^2 represents a diffusive smoother (three points in this 1D model, in which case $\Delta^2 u_i = u_{i-1} - 2u_i + u_{i+1}$); and the weighting coefficients in (2.4) are given by[1]

$$w_{1n} = \frac{W}{\Delta t}\left(\frac{1+N-n}{N}\right) \qquad n = 1, 2, \ldots, N, \tag{2.5}$$

and $w_{2n} = 0.2w_{1n}$. The coefficient W in (2.5) is referred to in this paper as the "sponge weight"; WRF sets this to 0.1, which is the value we use unless otherwise specified. In this study, $N = 5$ unless otherwise stated. This follows the example of Moeng et al. (2007), who needed five points to get acceptable results for their two-way nested large eddy simulations of the planetary boundary layer. In contrast, WRF by default uses only three sponge points, although this can be changed by the user.

The implementation of the sponge BC uses explicit forward differencing to evaluate the sponge terms in (2.4). The Δt in the denominator of (2.5) cancels out when the timestep is taken, ensuring that the amount of effective dissipation performed during a timestep is independent of its length. In our test cases, the sponge zone is added to the ends of the domain, so that the size of the interior region is identical for both BCs. When using the interpolation BC, the u boundary points are specified directly from

---

[1] The expression for the sponge weights in the WRF documentation is slightly different than that given in (2.5). The expression in Skamarock et al. (2005) produces a weight of zero for the innermost point of the sponge zone (called the "relaxation zone" in WRF), and so the true width of the sponge zone is one grid point less than that specified by the user. Here, we have altered the expression so that every point in the sponge zone has a nonzero weight, but that the weights are the same for the N sponge points as they would be if WRF was set to use $N+1$ points.

the coincident coarse-grid points, while the h boundary points, which do not coincide with coarse-grid points on this staggered grid, are linearly interpolated to from the coarse grid. Linear interpolation is also used for all boundary and sponge-zone points when the sponge BC is used. Tests with the interpolation BC showed little change in the amplitude of reflected waves to the choice of interpolation method.

In our simulations, the grids are aligned so that *all* of the coarse-grid points coincide with a nested-grid point, and so the additional step performed in two-way simulations of updating the coarse grid using the nested grid's data is performed by setting the values on the coarse-grid points to the values of the coincident nested-grid points. [Is there a degree of aliasing with this approach?—MTS] This differs from the approach used by Skamarock and Klemp (1993) and others, in which the update uses averages of nested-grid points. When the sponge BC is used, the sponge zone is not included in the update process.

The initial condition (IC) used here consists of a Gaussian-modulated sinusoidal wave of a given wavelength λ specified on the nested grid, and then updated to the coarse grid (regardless of whether one-way or two-way nesting is used). The value of $u(x, 0)$ is chosen so that there is a single eastward-moving wave and the westward characteristic is set to zero. The IC is thus:

$$h(x, 0) = \cos\left((x - x_0)k\right) \exp\left((x - x_0)^2/\sigma\right)$$

$$u(x, 0) = \frac{g}{c} h(x, 0),$$

where $x_0 = L_{xc}/2 = 8$ km, $k = 2\pi/\lambda$ is the wavenumber, and $\sigma = 5.333(\mathrm{km}^2)$. An example IC is seen in Fig. 2.1a.

2.2 Simulation Results

2.2.1 Waves of intermediate wavelength on the coarse grid

We begin by considering waves that are moderately-well resolved on the coarse mesh and very well resolved on the fine mesh. Fig. 2.1 compares the behavior of one-way and two-way nesting, along with the performance of both interpolation and sponge BCs when a $\lambda = 36\Delta x_n$ shallow-water wave ($12\Delta x_c$ on the coarse grid) encounters the boundary of the fine mesh. The initial condition on the nested grid is shown in Fig. 2.1a. The next four panels show the solution at a time when it has propagated through the right boundary and any reflected wave has returned to the center of the nested grid. Clearly one-way (gray lines) nesting performs worse than two-way nesting (black lines), and the interpolation BC creates more reflection than the sponge. The amplitudes of the reflected waves shown in Fig. 2.1b–e are given as percentage of their initial amplitudes in the first line of Table 2.1. These numerical values confirm the superiority of both two-way nesting and the sponge BC for this wavelength.

As shown by the next two lines in Table 2.1 the reflection becomes more severe as the wavelength is decreased, although for one-way nesting the increase is not a monotone function of the wavelength. In the one-way case, the reflections produced by the $18\Delta x_n$ wave are similar to those generated in the $36\Delta x_n$, while the behavior of the $24\Delta x_n$ is far worse. The reason the reflection for the $18\Delta x_n$ wave is reduced relative to that for the $24\Delta x_n$ wave will be discussed in Section 3a.

The behavior of the reflected modes in the shallow-water system is different from that produced at the nested grid boundary by numerical approximations to the 1D advection equation for a scalar concentration ϕ with constant background wind speed c,

$$\frac{\partial \phi}{\partial t} + c\frac{\partial \phi}{\partial x} = 0.$$

If the preceding is discretized using leapfrog time differencing and second-order centered space differencing

$$\delta_{2t}\phi + c\delta_{2x}\phi = 0, \tag{2.6}$$

the only modes with negative group velocities, and therefore the only modes capable of transporting reflected waves away from the downstream boundary have wavelengths in the range $2\Delta x_n \leq \lambda < 4\Delta x_n$ (Durran, 1999, Sec. 2.4.1). This is illustrated in Fig. 2.2

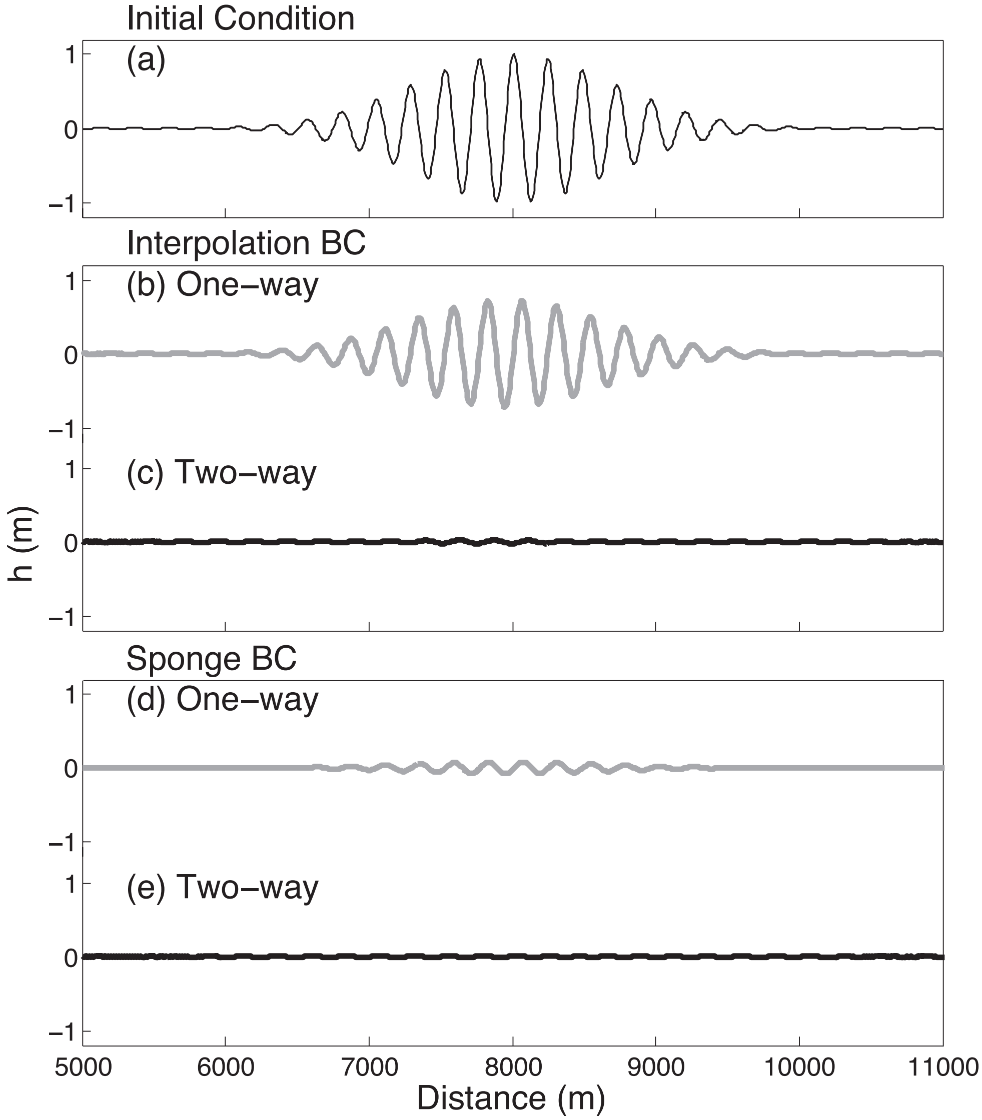

Figure 2.1: Nested-grid solutions for $h(x,t)$ in simulations of the 1D shallow-water model. (a) shows the initial condition (thin solid line) which is an eastward-propagating $\lambda = 36\Delta x_n$ wave packet. (b)–(e) depict the solution at $t = 1250$ s after any reflection has returned to the center of the nested grid. Interpolation BC results are shown for one-way (b) and two-way nesting (c). Sponge BC results for one-way nesting are in (d) and two-way nesting in (e). Results from one-way nesting are shown in gray.

for one-way nesting, the interpolation BC, and an incident $36\Delta x_n$ wave packet moving at $c = 5$ m s^{-1}. Fig. 2.2a shows the packet at the initial time, Fig. 2.2b shows the reflection after it propagates back to the center of the nested mesh as a high-amplitude mode of wavelength approximately $2\Delta x_n$.

Reflections into such short waves are easily removed by applying artificial dissipation. Suppose fourth-order dissipation of the form

$$\frac{\gamma_4}{16\Delta t}\left(-\phi_{j-2} + 4\phi_{j-1} - 6\phi_j + 4\phi_{j+1} - \phi_{j+2}\right) \tag{2.7}$$

is added globally to the right-hand side of (2.6) when evaluating the value of ϕ_j at the next time level, where j represents the solution at $x = j\Delta x$. Using only a very weak dissipation coefficient (γ_4) of 0.01—an order of magnitude less than that used in many mesoscale models (cf. Knievel et al., 2007)—easily eliminates the reflected modes (Fig. 2.2c). For a $2\Delta x_n$ wave, this γ_4 yields an e-folding time for the wave amplitude of 53 s, or $0.017 L_{xc}/c$. More generally, when reflections are comprised of very short wavelength modes, they will almost immediately be removed by the background dissipation present in nearly all mesoscale models.

On the other hand, in systems that support waves moving in both directions, such as the shallow-water equations, reflections often appear as spurious physical modes that are not easily removed by artificial dissipation because the magnitude of any artificial dissipation is normally set low enough that is does not significantly impact most physical modes. For example, adding significant dissipation (with $\gamma_4 = 0.1$) to the staggered shallow-water model and comparing the $36\Delta x_n$ case to that without dissipation, we see from Table 2.1 that even such relatively strong dissipation exerts only a modest influence on the amplitude of this very well-resolved reflected wave. This wave is damped with an e-folding time of approximately $7L_{xc}/c$, so there is very little reduction of the amplitude of either the incident wave or of the reflection; instead, the artificial dissipation is damping out the sharp discontinuity caused by the interpolation BC when the two solutions are out of phase, thereby reducing the

	Interpolation BC		Sponge BC	
IC Wavelength	One-way	Two-way	One-way	Two-way
$36\Delta x_n$	76%	2.4%	8.5%	0.02%
$24\Delta x_n$	186%	5.4%	20.%	0.38%
$18\Delta x_n$	90.%	10.%	9.9%	0.94%
$36\Delta x_n$, $\gamma_4 = 0.1$	47%	2.1%	7.3%	0.18%
$9\Delta x_n$	107%	96%	19%	44%

Table 2.1: Reflection amplitudes for various initial conditions and BCs in the 1D shallow-water model. Simulations use no damping of the form (2.7) unless otherwise specified.

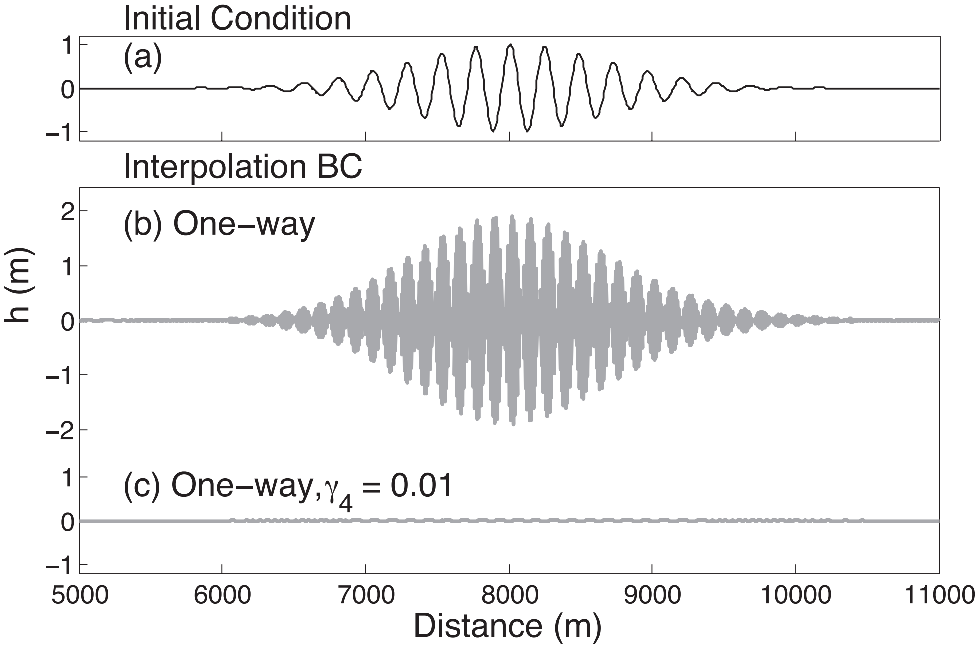

Figure 2.2: Simulation of a $36\Delta x_n$ wave in the scalar advection equation with a one-way nest and the interpolation BC. (a) Initial condition; (b) at $t = 1300$ s, no dissipation; (c) at $t = 1300$ s with fourth-order dissipation applied, $\gamma_4 = 0.01$. The thickness of the line in (b) obscures the $2\Delta x_n$ wavelength of the reflected mode.

amplitude of the reflected wave. Repeating this case with dissipation applied only at the two gridpoints nearest to the boundary yielded a reflection with a similar amplitude to a simulation with global dissipation, confirming this explanation.

Fig. 2.3a depicts the amplitude of the reflected wave as a function of the wavelength of the incident disturbance for the interpolation BC. Here, the reflections are given in terms of the "normalized reflection amplitude",

$$\frac{\max|h_{rn}|}{h_0} \tag{2.8}$$

where h_{rn} represents the value of $h(x,t)$ on the nested grid after the disturbance has been reflected and returned to the interior of the nested grid, and h_0 represents the initial amplitude of the outgoing disturbance. Again, the two-way nest (pluses) produces substantially lower-amplitude reflections than the one-way nest (crosses) for all but the shortest wavelengths. In fact, when using the interpolation BC the reflected wave's amplitude for a $12\Delta x_n$ disturbance on a two-way mesh is roughly the same as that of a $48\Delta x_n$ disturbance on a one-way mesh! Using the sponge BC (Fig. 2.3b) reduces the errors in one-way nesting by as much as a factor of ten for some wavelengths, but one-way nesting still produces much larger reflections than does two-way nesting for wavelengths $\geq 12\Delta x_n$.

2.2.2 Poorly-resolved waves on the coarse grid

While for moderately-well resolved waves two-way nesting is superior, this is not the case for more poorly-resolved disturbances. When using the interpolation BC, the amplitude of the reflected wave is equal to that of the incident wave for wavelengths $\leq 9\Delta x_n$ for both one-way and two-way nesting (Fig. 2.3a). The sponge BC (Fig. 2.3b) again reduces the amplitude of the reflections for these short wavelengths, but is much more effective for one-way nesting than for two-way nesting.

The $9\Delta x_n$ case (Fig. 2.4a; see also Table 2.1) illustrates these behaviors. Using the interpolation BC (Fig. 2.4b), reflection is nearly total in the one-way case, and

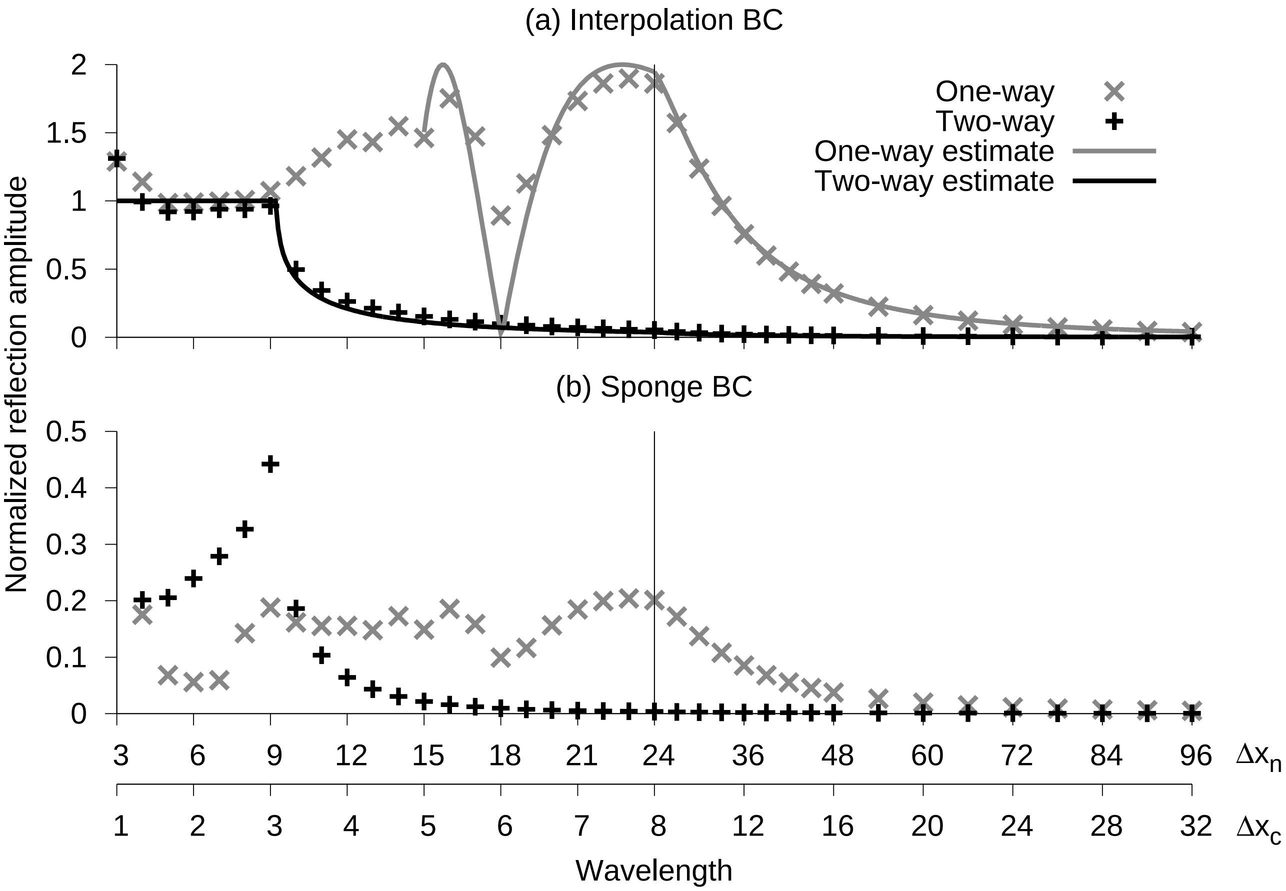

Figure 2.3: One-way vs. two-way nesting in the 1D shallow-water model at time 1200 s. (a): normalized reflection amplitude (2.8) as a function of wavelength for the interpolation BC; (b) for the sponge BC. Note change in vertical scale in (b) and change in horizontal scale in both panels at $24\Delta x_n$. Solid lines in (a) refer to the estimates (2.9) and (2.11) for the reflection amplitudes.

is only slightly reduced in the two-way simulation (Fig. 2.4c). Using the sponge BC, the reflected mode is substantially reduced with one-way nesting (Fig. 2.4d), but is almost half the amplitude of the incident wave in the two-way case (Fig. 2.4e). Although one-way nesting produces reflections of similar- or lower-amplitude than does two-way nesting for this $9\Delta x_n$ disturbance, the one-way results are degraded by a spurious mode propagating into the nested grid from the outflow (right) boundary (Fig. 2.4bd).

The sudden shift in the behavior of the two-way nest's reflections when the wavelength of the incident wave drops to $9\Delta x_n$ (Fig. 2.3) is surprising. One might expect disturbances to become "trapped" on the coarse grid and to produce total reflection only when the numerical group velocity of the wave on the coarse grid is directed inward. For our staggered-grid discretization of the shallow-water equations, we expect that trapping should only occur for wavelengths $\leq 6\Delta x_n$ (or equivalently, $\leq 2\Delta x_c$).

2.2.3 Filtered sponge BC: an improvement to the sponge BC

A close examination of the coarse-grid solution provides both a reason for this behavior as well as a solution. For poorly-resolved solutions, there is a substantial difference in the amplitudes and wavelengths of the solutions on the two grids, causing a mismatch between the solutions and thus larger reflections; in particular, in two-way nesting there can be a large difference in the wavelength of the fine-mesh solution and that on the coarse mesh outside the region where the grids overlap. If such short-wavelength waves are indeed causing the problems, then filtering the coarse grid data to remove the problematic high-frequency modes before using it in the sponge BC should decrease the amplitude of the reflections. To this end, we introduce the "filtered sponge" BC, in which the coarse-grid fields u_c and h_c are smoothed with the fourth-order filter (2.7) before being used in (2.4). Note that this filter is applied only to the data being used as the coarse-grid values in the sponge zone and *does not alter the actual coarse-grid solution.* Here, $\gamma_4 = 1$, so that any $2\Delta x_c$ waves are eliminated with a single pass of the filter. We use the fourth-order filter because it is a simple scale-selective filter that efficiently damps short wavelengths while having little effect on better-resolved disturbances.

The response of the filtered sponge BC to an incident $9\Delta x$ wave is compared with the other nested BCs in Fig. 2.4. In the one-way case, when the wave packet encounters the filtered sponge BC the filter reduces the spurious radiation of waves inward through the downstream boundary, but otherwise has a relatively minor impact on the solution (Fig. 2.4f). In contrast, in the two-way case the filter substantially reduces the reflection (Fig. 2.4g) relative to that generated by the unfiltered sponge BC (Fig. 2.4e).

The magnitude of the reflections produced by the filtered sponge BC is compared with that for the standard sponge BC as a function of wavelength in Fig. 2.5. For two-way nesting and incident waves that are poorly resolved on the coarse grid ($< 12\Delta x_n$), filtering greatly reduces the reflections. (Compare the black crosses with the open black squares.) At longer wavelengths, the filtered sponge BC also outperforms the unfiltered sponge BC, although the both give very similar results for wavelengths longer than $20\Delta x_n$. In one-way nesting, the improvement produced by filtering is much smaller and is largely limited to wavelengths between 8 and $11\Delta x_n$. (Compare the gray crosses with the open gray diamonds.)

2.3 Analysis of reflections generated by the interpolation BC

2.3.1 One-way nesting

The reflection generated at the nested-grid boundary using one-way nesting is strongly influenced by any difference in the phase of the wave on the coarse and nested grids in the neighborhood of the nested-grid boundary.[2] Such differences are illustrated for a $24\Delta x_n$ wave in Fig. 2.6a, in which the coarse- and nested-grid waves from a one-way

---

[2] Elsberry (1978) noted that reflections in one-way nesting could be caused by the solutions moving out of phase between the two grids, although he did not elaborate on this idea.

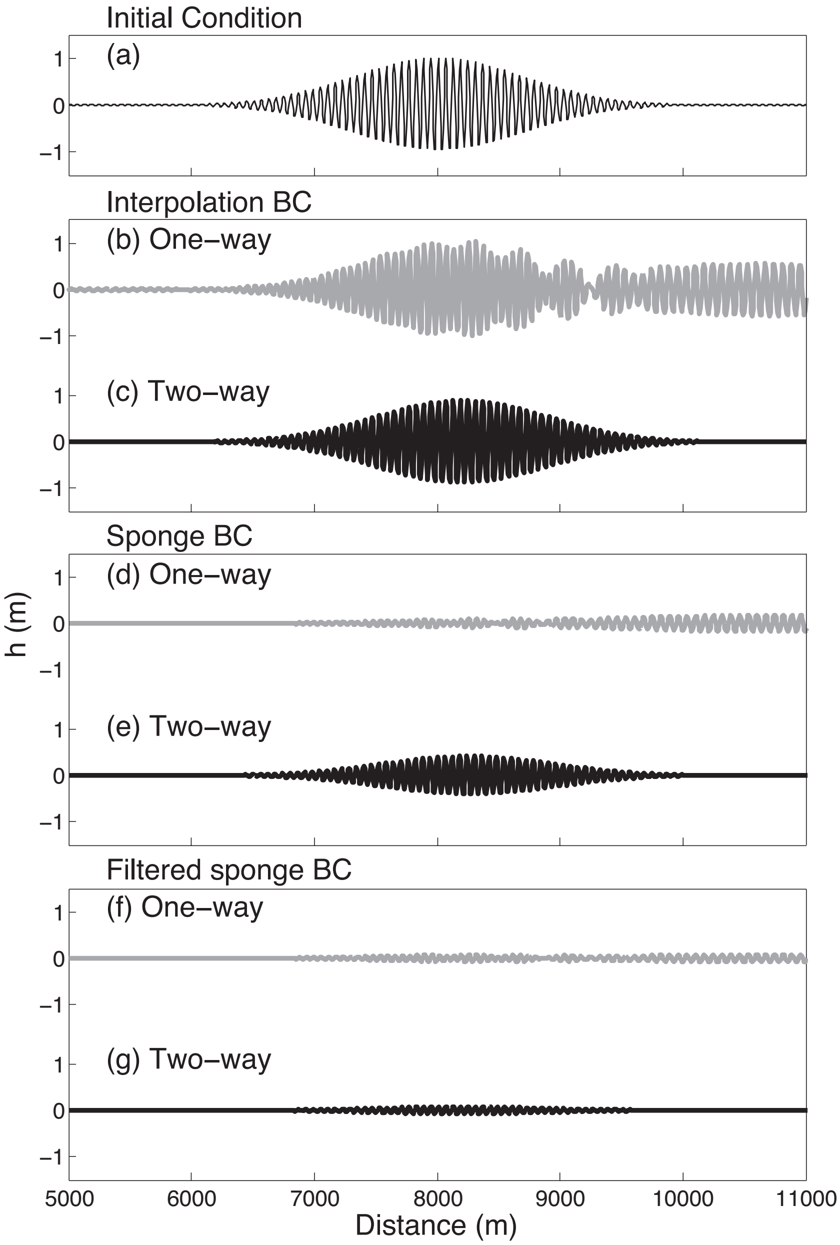

Figure 2.4: As in Fig. 2.1, but for the 1D shallow-water model with a $9\Delta x_n$ wave. Panels (f) and (g) show results using the filtered sponge BC described in Section 2.2.2.

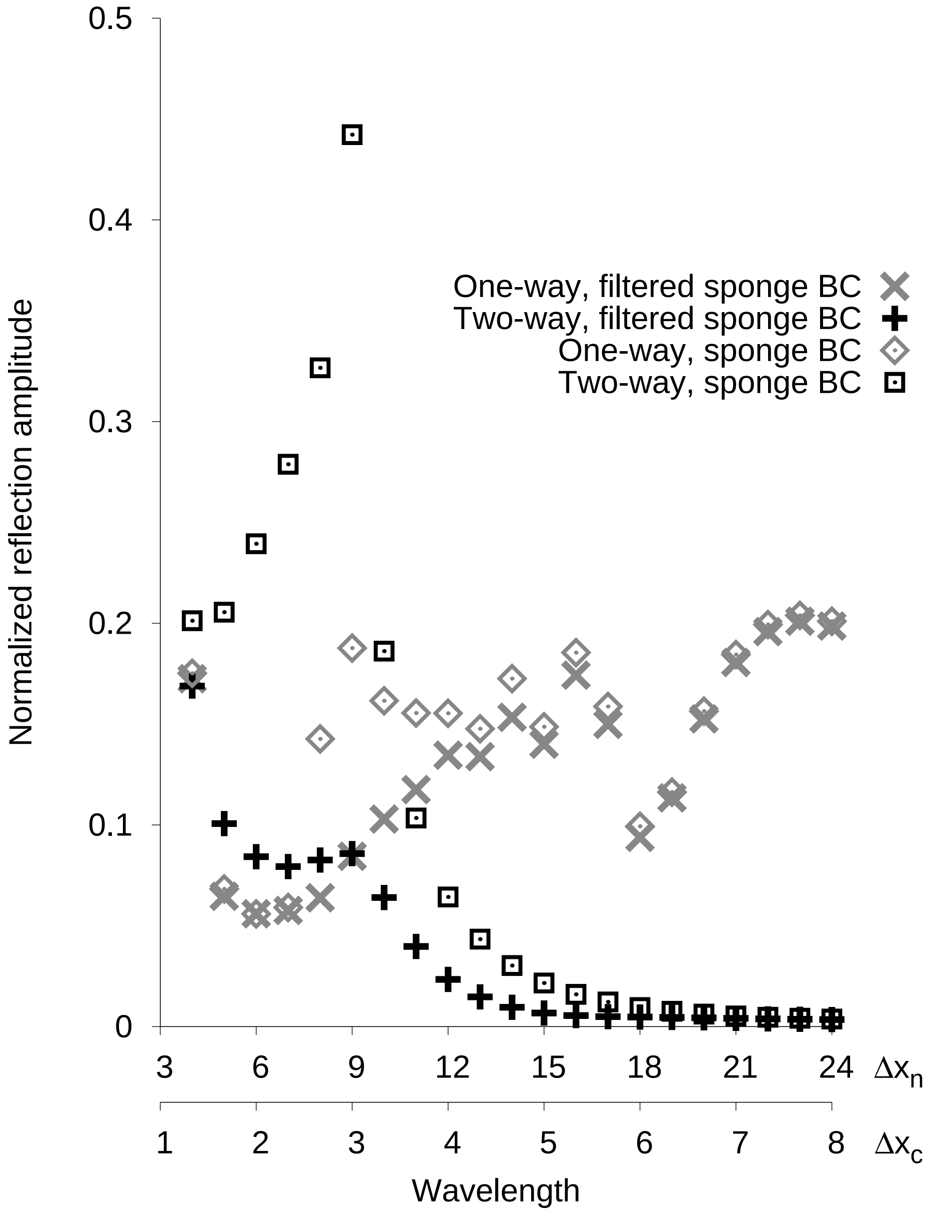

Figure 2.5: Comparison of normalized reflection amplitudes for simulations of the 1D shallow-water model using the sponge BC with and without filtering.

simulation are both plotted in the region near the original nest boundary, although for these simulations, the actual nest boundary has been moved far beyond the right edge of the plot. Due to numerical dispersion and the difference in resolution of the wave on the coarse and nested grids, the phase speed of the wave on the coarse grid is slower than that on the nested grid.

The difference in numerical phase speeds between the two grids is relatively small for the $24\Delta x_n$ wave; however, in the one-way case, the difference in phase accumulates as the waves propagate toward the nested grid boundary, so that for the particular dimensions of the nested grid used here, the coarse and nested solutions are nearly half a wavelength out of phase when the packet arrives at the boundary (Fig. 2.6a), yielding the maximum amount of reflection. The difference in phase speeds on the coarse and nested grids is larger for a $18\Delta x_n$ wave, yet counterintuitively smaller reflections are produced because for the domain size we are using, the $18\Delta x_n$ waves come back into phase by the time the center of the wave packet reaches the boundary (Fig. 2.6b). Small reflections nevertheless occur in the $18\Delta x_n$ case because at earlier or later times, when the wave amplitude at the boundary is lower, there is some difference in phase between the solutions on the two grids.

Theoretical estimates for the interpolation BC's errors in one-way nesting can be derived as a function of the computational phase speeds on each grid. If we neglect the amplitude modulation of the wave packet, we can easily determine the reflection r_{1w} produced solely by the phase difference in the carrier wave on each grid. Suppose unit-amplitude monochromatic waves of the same wavelength $(2\pi/k)$ are in phase on the coarse and nested grids at time $t = 0$, and assume the interpolation BC is imposed at some point $x = L$ (which we will take to be the boundary of the nested grid). The interpolation BC will generate a reflected wave of amplitude r_{1w} and wavenumber $-k$ on the nested grid, and the matching condition at $x = L$ becomes

$$\exp(ikL - i\omega_n t) + r_{1w} \exp(-ikL - i\omega_n t) = \exp(ikL - i\omega_c t),$$

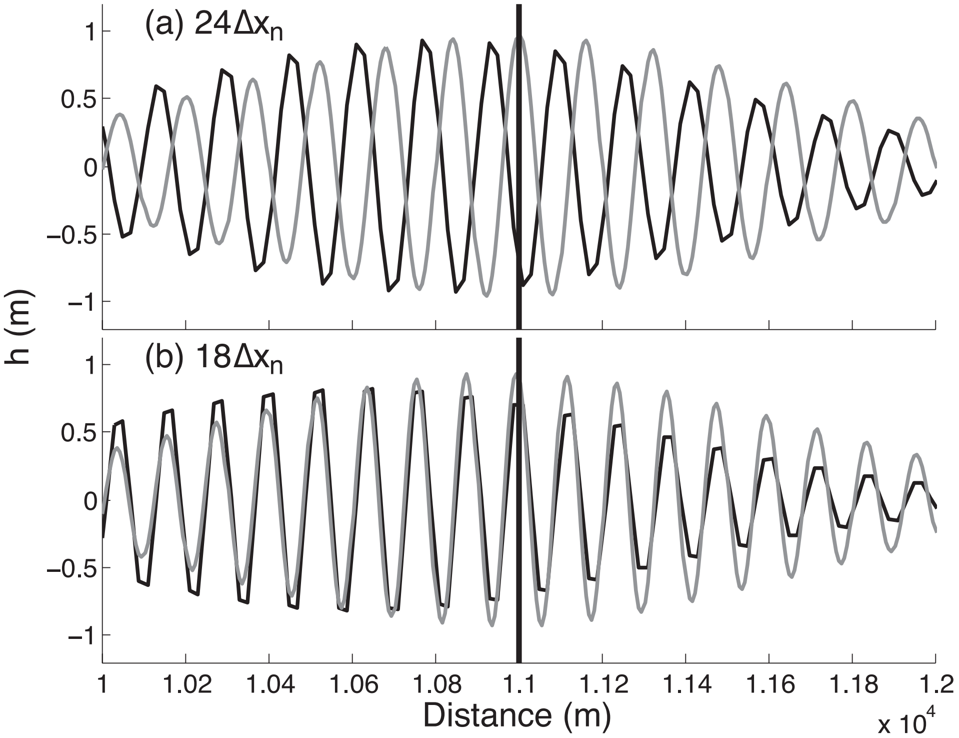

Figure 2.6: Nested- (gray) and coarse-grid (black) solutions for shallow-water simulations in which the eastern boundary of the nest is moved from 11 to 15 km. (a) $24\Delta x_n$ and (b) $18\Delta x_n$ waves at $t = 600$ s, at which time the fine-mesh wave packet is centered around the previous location of the nested-grid boundary (indicated by the heavy vertical line at $x = 11$ km.)

where $\omega_n(k)$ and $\omega_c(k)$ are the frequencies on the nested and coarse grids as given by the discrete dispersion relation.

Solving for r_{1w} yields:

$$r_{1w} = \exp(i\omega_n t)\exp(2ikL)\left[\exp(-i\omega_c t) - \exp(-i\omega_n t)\right],$$

or

$$|r_{1w}| = \left|\exp(-iw_c t) - \exp(-i\omega_n t)\right|.$$

Using the relationships $\omega_n = c_n k$ and $\omega_c = c_c k$ for the phase speeds c_n and c_c on the nested and coarse grids, the amplitude of the reflected wave being produced at time t may be expressed

$$|r_{1w}| = \sqrt{2}\left[1 - \cos\left(k\left(c_n - c_c\right)t\right)\right]^{1/2}, \tag{2.9}$$

where, for our staggered grid approximation to the shallow-water equations in the limit of good time resolution ($c\Delta t/\Delta x \ll 1$),

$$c_n = \frac{2c}{k\Delta x_n}\sin\left(\frac{k\Delta x_n}{2}\right) \qquad c_c = \frac{2c}{k\Delta x_c}\sin\left(\frac{k\Delta x_c}{2}\right). \tag{2.10}$$

In our simulations, t is chosen to be the time when center of the nested-grid wave packet reaches the boundary.

2.3.2 Two-way nesting

A similar analysis can be performed for two-way nesting. Vichnevetsky (1981) derived the expression

$$r_{2w} = \frac{c_{gn} - c_{gc}}{c_{gn} + c_{gc}} \tag{2.11}$$

for reflection at a grid refinement as a function of the numerical *group* speeds[3] c_{gn}, c_{gc} on the nested and coarse grids, respectively. Since wave propagation back and forth across the nest boundary in a two-way nest is very similar to that for a grid refinement, we will use the same expression as an estimate of the expected reflection

---

[3] Defined as $\partial\omega/\partial k$, where ω is the frequency from the computational dispersion relation.

amplitude of a unit-amplitude disturbance at the nested-grid boundary when using a two-way nest and the interpolation BC.

The derivation of (2.11) uses the assumption that the frequencies (not wavenumbers[4]) of the waves on the two grids match; thus, the wavenumber k_c of the coarse-grid solution is that which satisfies

$$c_n k = c_c k_c, \tag{2.12}$$

where k is the wavenumber on the nested grid which is specified by the initial condition. For the staggered-grid second-order spatial discretization used here, (2.12) implies

$$\sin\left(\frac{k_c \Delta x_c}{2}\right) = \frac{\Delta x_c}{\Delta x_n} \sin\left(\frac{k \Delta x_n}{2}\right). \tag{2.13}$$

As the wavelength on the nested grid decreases, the right-hand side of (2.13) will exceed unity and k_c will become complex-valued, implying that the coarse-grid solution will be evanescent. For $\Delta x_c/\Delta x_n = 3$ evanescence is predicted to occur for nested grid wavelengths $\leq 9\Delta x_n$, although numerical tests show that the longest nested grid wavelength which is transmitted into an evanescent wave is approximately $8.5\Delta x_n$. The coarse-grid solution for this wave is shown in Fig. 2.7; here, the amplitude of the evanescent disturbance is greatest at 638 s because this is when the center and most intense part of the wave packet arrives at the nested-grid boundary. For all evanescent coarse-grid disturbances, the real part of k_c is $\pi/2$, corresponding to a $2\Delta x_c$ wave. The imaginary part of k_c is smallest, and the e-folding distance on which the wave decays is largest, for a wavelength just short enough to cause evanescence.

We may now use Vichnevetsky's expression (2.11) for reflections in two-way nesting

---

[4] The solutions in a two-way nested simulation are held identical over the update region (the region where the two grids coincide, sponge zones excepted), and so the coarse-grid wavelength can only change when the solution propagates out of the update region. In contrast, in one-way nesting the coarse-grid solution is initialized to and remains the same wavelength as that on the nested grid.

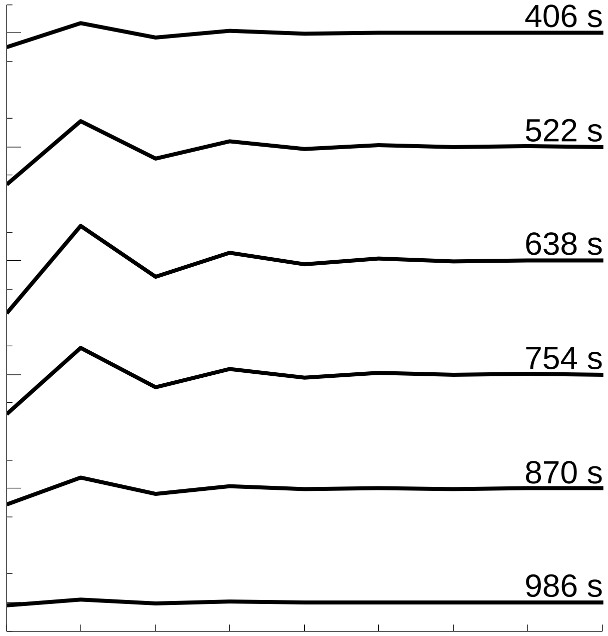

Figure 2.7: Coarse-grid two-way nested shallow-water model solutions at various times for a $8.5\Delta x_n$ wave. Left edge of plot represents first point on coarse grid which is not updated from the nested grid. Horizontal tick interval is one coarse-grid interval; vertical tick interval is 1 m, with elongated marks representing 0.

where, for our discretization, the group velocities are

$$c_{gn} = c\cos\left(\frac{k\Delta x_n}{2}\right) \qquad c_{gc} = c\cos\left(\frac{\mathrm{Re}\left(k_c\right)\Delta x_c}{2}\right) \tag{2.14}$$

Note that evanescent coarse-grid solutions have a group velocity of 0, so $r_{2w} = 1$ and we expect total reflection.

2.3.3 Comparison with numerical results

The amplitude of the reflections estimated from (2.9) and (2.11) are compared with the results from simulations with the interpolation BC in Fig. 2.3a. Except for waves shorter than $20\Delta x_n$ (which corresponds to a only moderately-resolved $6.7\Delta x_c$ wave on the coarse grid), the agreement between (2.9) and the one-way numerical simulations is quite good; and for all wavelengths the agreement between (2.11) and the two-way numerical simulations is very good. We conclude from this that the reflections in the one-way interpolation case can be interpreted as arising from the differences in the phase of the wave on the coarse and nested grids, and that reflections in the two-way interpolation case arise from differences in the group velocity. In the case of the one-way interpolation BC, the errors in the estimates for shorter wavelengths appear because (2.9) does not take into account the finite width of the packet. The range of phase differences that occur over the width of the packet increases as the difference between the phase speeds on the coarse mesh increases, which in turn increases as the wavelength of the carrier wave decreases. Although (2.9) is based solely on the phase difference when the center of the packet reaches the boundary, reasonable qualitative agreement is seen in Fig. 2.3a down to $15\Delta x_n$ ($5\Delta x_c$), below which the theoretical value becomes highly oscillatory (and so is not plotted). The two-way estimate (2.11) correctly predicts very small reflections for wavelengths larger than $24\Delta x_n$ ($8\Delta x_c$) and accurately predicts the simulated reflections through the smallest wavelengths, including the total reflection occurring for wavelengths $\leq 9\Delta x_n$.

The difference in the group velocities on the fine and coarse meshes for packets with wavelengths of $9\Delta x_n$ or shorter is large enough that, on a one-way mesh, the nested-grid packet attempts to pass through the boundary before the coarse-grid packet has even arrived. As a consequence, the coarse-grid values imposed at the nest boundary are almost zero, and the interpolation BC generates almost total reflection. Further, once the coarse-grid solution reaches the nested grid's boundary, the BC will radiate the coarse-grid solution back onto the nested grid, creating the incoming disturbance seen in Fig. 2.4b.

2.3.4 Implications for the sponge BC

The sponge BC causes lower-amplitude reflections than does the interpolation BC, but for well-resolved wavelengths behaves similarly to the interpolation BC with respect to changes in the solution's wavelength (Fig. 2.3): two-way nesting yields small but progressively larger reflections with decreasing wavelength, and one-way nesting has peaks in reflection amplitude at 24 and $16\Delta x_n$ with a local minimum in between. More prominent qualitative differences between the behavior of the two BCs are found for poorly-resolved wavelengths. When using the sponge BC and a one-way nest, wavelengths $\leq 9\Delta x_n$ are damped towards the zero coarse-grid solution, causing the sponge BC to act as a damping layer and thus substantially reducing the amplitude of the reflections. However, much like the interpolation BC the sponge BC creates an incoming disturbance (Fig. 2.4d) once the coarse-grid solution reaches the nested-grid boundary. This is mitigated by the use of the filtered sponge BC (Fig. 2.4f), which damps the poorly-resolved coarse-grid data before applying it to the nested-grid solution in the sponge zone.

The high-frequency coarse-grid modes appearing for marginally-well-resolved solutions in two-way nesting can degrade the sponge BC by creating a mismatch in the sponge zone, so that the BC fails to appropriately damp the outgoing nested grid solution. This is particularly pronounced at $9\Delta x_n$ (Fig. 2.4e), which transmits into a slowly-propagating mode with a wavelength slightly longer than $2\Delta x_c$. This disturbance greatly differs in wavelength from the nested grid solution, while also having a larger amplitude than the evanescent solutions and failing to decay away from the nested-grid boundary. Hence, the $9\Delta x_n$ two-way case causes a coarse-grid solution which interferes the most with the sponge BC and causes the greatest reflection compared to other wavelengths. The effectiveness of the filtered sponge BC (Figs. 2.4g, 2.5) verifies these assertions: if these interfering coarse-grid disturbances are filtered out, the reflections in two-way nested simulations are greatly reduced.

2.4 Generalizing the preceding results

2.4.1 Other finite difference schemes

The formulas (2.9) and (2.11) for the amplitudes of reflected waves may also be applied to other numerical schemes and other problems involving wave propagation. For the interpolation BC, the key factor governing reflections on one-way nests is the difference between the phase speeds on the coarse and fine meshes; for two-way nests, the key factor is the difference in group velocities. Both differences are typically smaller on a staggered grid than on an unstaggered mesh. Higher order methods generally give more uniform (and more accurate) approximations to the phase speeds of all but the very shortest waves with wavelengths less than about $3\Delta x$. At least for longer waves, higher order methods also tend to increase the uniformity in the approximation of the group velocity.

As a concrete example, consider how the differences between the phase speeds and group velocities in numerical approximations to the linearized shallow-water system (2.1)–(2.2) are influenced by switching between staggered and unstaggered meshes and between second- and fourth-order centered spatial differences. Using second-order spatial differencing on an unstaggered grid yields the scheme

$$\begin{aligned} \delta_{2t}u + g\delta_{2x}h &= 0 \\ \delta_{2t}h + H\delta_{2x}u &= 0. \end{aligned}$$

In the limit of good time resolution ($c\Delta t/\Delta x \ll 1$), the numerical phase speed and group velocities for this scheme are

$$c_{2U} = \frac{c}{k\Delta x_c}\sin\left(k\Delta x_c\right) \quad \text{and} \quad c_{g_{2U}} = c\cos\left(k\Delta x_c\right). \tag{2.15}$$

Fourth-order spatial differencing on an unstaggered grid gives the method

$$\begin{aligned} \delta_{2t}u + g\left(1 - \frac{(\Delta x)^2}{6}\delta_x^2\right)\delta_{2x}h &= 0 \\ \delta_{2t}h + H\left(1 - \frac{(\Delta x)^2}{6}\delta_x^2\right)\delta_{2x}u &= 0, \end{aligned}$$

for which (assuming $c\Delta t/\Delta x \ll 1$)

$$c_{4U} = \frac{c}{6k\Delta x}\left(8\sin k\Delta x - \sin 2k\Delta x\right) \quad \text{and} \quad c_{g_{4U}} = \frac{c}{3\Delta x}\left(4\cos k\Delta x - \cos 2k\Delta x\right). \tag{2.16}$$

Finally, the scheme

$$\begin{aligned} \delta_{2t}u + g\left(1 - \frac{(\Delta x)^2}{24}\delta_x^2\right)\delta_{x}h &= 0 \\ \delta_{2t}h + H\left(1 - \frac{(\Delta x)^2}{24}\delta_x^2\right)\delta_{x}u &= 0, \end{aligned}$$

is a fourth-order spatial discretization on a staggered grid. In the limit of good time resolution the phase speed and group velocity for this scheme satisfy

$$\begin{aligned} c_{4S} &= \frac{2c}{k\Delta x}\left[\frac{9}{8}\sin\left(\frac{1}{2}k\Delta x\right) - \frac{1}{24}\sin\left(\frac{3}{2}k\Delta x\right)\right] \\ c_{g_{4S}} &= \frac{c}{8}\left[9\cos\left(\frac{1}{2}k\Delta x\right) - \cos\left(\frac{3}{2}k\Delta x\right)\right]. \end{aligned} \tag{2.17}$$

In the case of one-way nesting, the actual reflections produced in a specific situation depend on the difference in the phase of the waves on the coarse and fine meshes at the fine-mesh boundary. This is a function of the distance to the boundary as well as the difference in the phase speeds on each mesh. Nevertheless, the larger the difference in the phase speeds, the more quickly the waves get out of phase and, in general, the larger the reflection that will be produced at a “nearby” boundary. Thus in Fig. 2.8 we characterize the potential of the preceding schemes to produce reflections by plotting the difference in phase and group velocities between the nested and coarse grids assuming a 3-to-1 grid refinement. In the one-way case (Fig. 2.8a), the coarse- and fine-mesh waves stay in phase better using staggered meshes and fourth-order schemes.[5] If for simplicity we neglect the difference in wavenumber between the two grids, the situation for two-way nesting (Fig. 2.8b) is roughly similar except that there is a much broader range of short waves for which fourth-order unstaggered differencing creates larger group-velocity differences than the second-order unstaggered approach. Numerical simulations have verified that the preceding methods do indeed produce reflections whose amplitudes vary from scheme to scheme in a manner consistent with the phase-speed and group-velocity differences shown in Fig. 2.8.

Of course the phase speeds and group-velocities are also influenced by the time differencing. Leapfrog time differencing accelerates the phase whereas centered space differencing decelerates the phase. If leapfrog time differencing is combined with second-order centered space differencing on an unstaggered grid, the phase errors in the resulting method tend to cancel, and they approach zero as $c\Delta t/\Delta x \to 1^-$. For the other three schemes considered in the preceding analysis, the net phase-speed and group velocity errors are more complicated functions of the Courant number and the wavelength, although they could nevertheless be evaluated in specific cases if so desired.

2.4.2 Effect of nested grid width

If the width of a *one-way* nested grid is changed, but the initial location of the wave packet is unchanged so that the wave takes a different amount of time to reach the boundary, the difference in phase between the solutions should also change, in which case (2.9) implies that the amplitude of the reflections should be different. Conversely,

---

[5] The sole exceptions are waves shorter than about $7\Delta x_n$ for which the differences in phase speed for the fourth-order unstaggered scheme exceed those for the second-order unstaggered method.

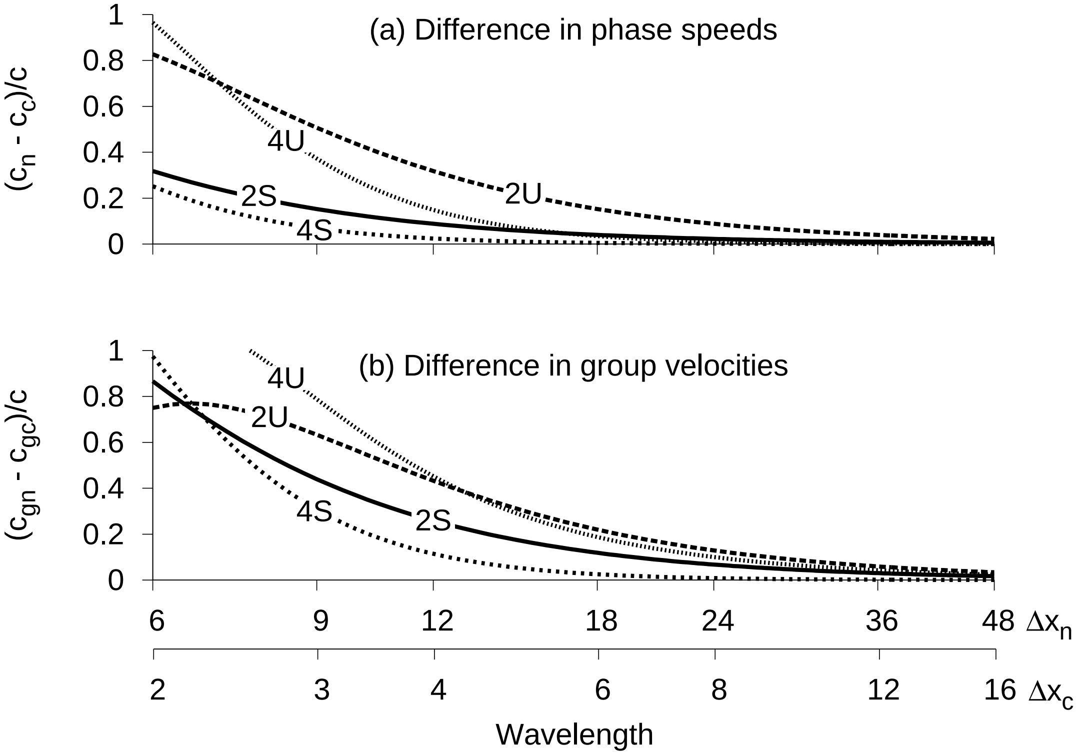

Figure 2.8: Difference between the nested- and coarse-grid (a) phase and (b) group velocities for several numerical schemes and grid setups for solving the shallow-water system, presuming a 3-to-1 grid refinement: second-order in space on a staggered grid (2S; Eqns. 2.10, 2.14), second-order in space on an unstaggered grid (2U; Eqn. 2.15), fourth-order in space on an unstaggered grid (4U; Eqn. 2.16), and fourth-order in space on a staggered grid (4S; Eqn. 2.18). Speeds are computed in the limit of good time resolution. Here, c is the true shallow-water wave speed $\sqrt{gH}$. In (b) the group-speed difference for 4U exceeds unity for coarse-grid wavelengths shorter than $8\Delta x_n$.

we expect that no such sensitivity to the width of the nested grid should be evident in a two-way nest, since the solutions remain in sync and the reflections are due to the changes in group velocity between the grids. To test this, a series of simulations has been performed in which the position of the eastern end of the nested grid is moved. The initial disturbance remains centered in the same location, so the time required for the packet to reach the boundary will be proportional to the width of the domain.

Fig. 2.9 shows the amplitude of the reflected mode for $24\Delta x_n$ waves in a one-way nest of varying lengths. It is apparent that as the nested grid width changes, the reflection from the interpolation BC varies like a rectified sine wave. The minimum reflections occur where the waves are in phase at the boundary, although as discussed previously, (2.9) underestimates the actual reflection when the waves are perfectly superimposed because it does not account for the variation in phase that occurs while a wave packet of finite width passes through the boundary. The sponge and filtered sponge BCs greatly reduce the reflection on the one-way nest, with little difference between the two BCs at this wavelength, but still show sensitivity to the relative phases of the coarse and nested-grid waves at the boundary. On the other hand, the reflections generated using two-way nesting are independent of the size of the domain regardless of the BC used, consistent with the insensitivity of (2.11) to time or position. The two-way example plotted in Fig. 2.9 uses the interpolation BC; the reflections generated by the sponge or filtered sponge BC on the two-way grid would plot as zeros and are not shown.

The sensitivity of one-way nesting to grid width also extends to shorter wavelengths. The nested grid solution on a 4000 m wide one-way nested grid (not shown) using a $9\Delta x_n$ disturbance no longer outruns the coarse-grid solution, and the reflections are found to be larger than for the original grid width for all three BCs, although the increase is reduced by using the filtered sponge BC. Again, two-way nesting shows little sensitivity to grid width, and if the filtered sponge BC is used two-way nesting yields smaller reflections than one-way nesting for this grid width.

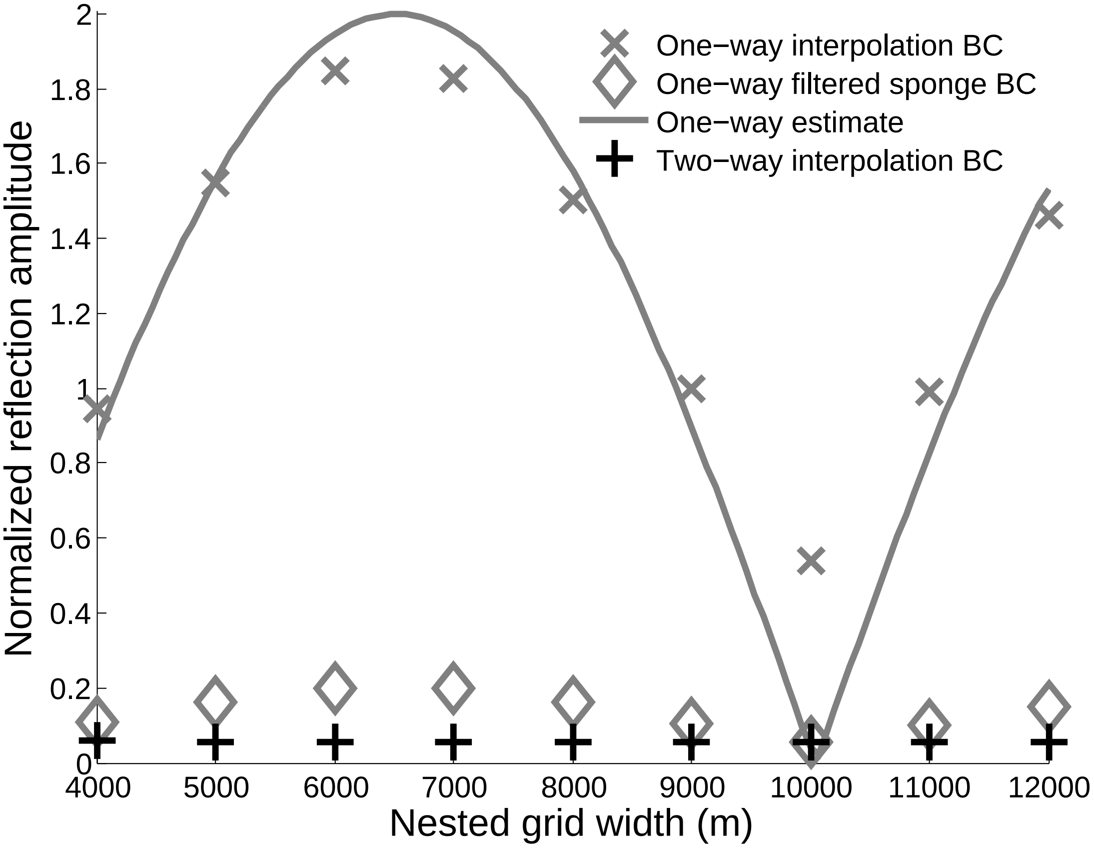

Figure 2.9: Normalized reflection amplitude (2.8) for $24\Delta x_n$-wavelength shallow-water disturbances as a function of the width of the nested grid. The solid line is the estimate (2.9) for the reflection in the one-way case. One-way reflection amplitudes for the sponge BC (not shown) are nearly identical to those for the filtered sponge BC.

2.4.3 Sensitivity of the Sponge BC

Is the relative performance of one-way and two-way nesting dependent upon the parameters defining the sponge BC? One might suppose that as the sponge zone becomes thicker, any reflection might be sufficiently reduced to the point where one-way and two-way nesting would perform similarly. To address this question, reflection amplitudes for a well-resolved $24\Delta x_n$ wave and a more poorly-resolved $9\Delta x_n$ wave are plotted as a function of the width of the sponge in Fig. 2.10 for both one-way and two-way nesting. For the $24\Delta x_n$ wave (Fig. 2.10a), two-way nesting is far superior to one-way nesting for sponge zones of any finite width (zero width corresponds to the interpolation BC), with the results differing little between the sponge or the filtered sponge BC. Indeed, the reflection on the one-way nest using a 15-point sponge is an order of magnitude larger than that on the two-way nest with only a three-point sponge. With the WRF default of three sponge points, the one-way nest yields a reflection almost a third of the size of the incident disturbance, while the two-way nest reduces the amplitude of the reflected mode to less than 1%.

As shown in Fig. 2.10b, the sponge BC performs poorly when a $9\Delta x_n$ wave encounters the boundary of a two-way nest. Somewhat better results may be achieved using the conventional sponge BC in a one-way nest, but much better results are obtained using the filtered sponge BC. The two-way filtered sponge BC generates less reflection than the other configurations except for very wide sponges where the reflections are negligible (note the logarithmic vertical scale).

We may also examine changing the sponge weight W in (2.5). If the weight is too small the BC would not effectively absorb the outgoing waves, while if it is too strong the BC would itself create reflections. Furthermore, since the coefficients are inversely proportional to Δt, taking a shorter timestep applies more damping over a given physical time and will thus alter the reflections off of the boundary. This line of thinking suggests that reflections should be dependent upon $W/\Delta t$, the rate at which the solution in the sponge zone is relaxed to that on the coarse grid. A series of tests were performed in which either W or the timestep were varied so that $W/\Delta t$ was modified from its original value of 0.25 s^{-1} to values in the range of 5×10^{-3} to 2.5 s^{-1}. For wavelengths in the range 18 to $36\Delta x_n$ (in which the filtered and sponge BCs yield nearly identical results) these tests found that two-way nesting still yielded smaller reflections than did one-way nesting for all cases, and for all but the smallest values of this ratio the amplitude of the reflection for two-way nesting was lower by an order of magnitude or more than that using one-way nesting. Similar tests for a $9\Delta x_n$ wave found that both nesting strategies yielded similar reflections when the filtered sponge BC was used regardless of the value of $W/\Delta t$.

2.5 Conclusions

We have compared the reflections of a wave packet of different wavelengths in both one-way and two-way nesting in a one-dimensional shallow-water model. Our results suggest that, in these idealized tests, two-way nesting is preferred to one-way nesting given its superiority for well-resolved waves, and that it is no worse than one-way nesting for poorly-resolved solutions if a filter is added to the sponge BC. Unsurprisingly, the sponge and filtered sponge BCs are seen to produce uniformly smaller reflections than the interpolation BC. Using artificial dissipation does not eliminate the reflections caused by one-way nesting in this shallow-water system, in which well-resolved solutions can propagate in either direction.

Reflections in two-way nesting are primarily caused by the shift in computational group velocities experienced by a disturbance attempting to cross from the nested to the coarse grid, which only becomes large for poorly-resolved solutions. Reflections in one-way nesting are primarily caused by the accumulation of phase errors between the two grids as a disturbance propagates across the nested grid, which causes a mismatch and reflection at the boundary even for solutions which are well-resolved on the nested grid. Two-way nesting keeps the two solutions in phase, and lacks the potentially-severe mismatch errors seen in one-way nesting.

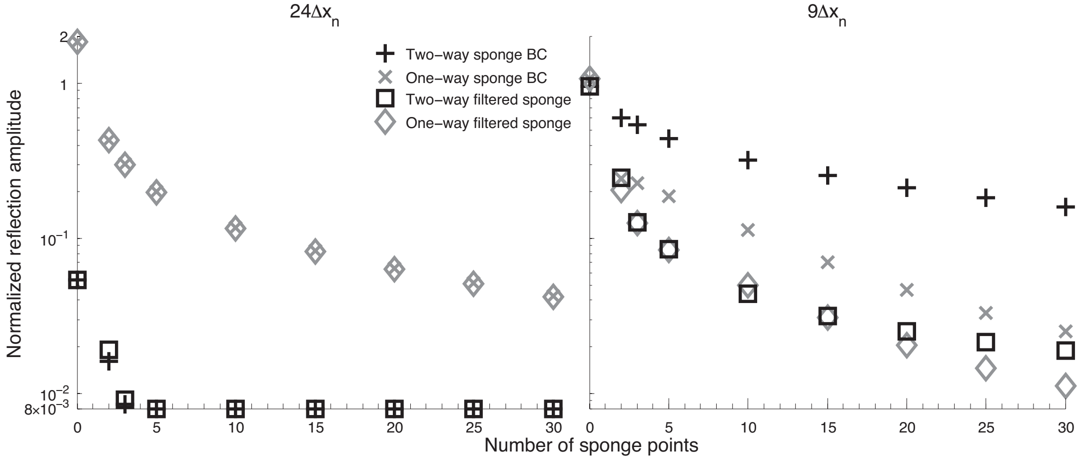

Figure 2.10: Normalized reflection amplitude (2.8) as a function of the number of sponge points for shallow-water disturbances of wavelengths 24 and $9\Delta x_n$. Reflection amplitudes below 8×10^{-3} are not shown. Note the logarithmic scale on the vertical axis.

Chapter 3

GENERALIZATION TO STRATIFIED SYSTEMS

The shallow-water model of the previous chapter demonstrated the unequivocal superiority of two-way nesting at preventing the reflection of localized disturbances. Does this result extend to more complicated systems of equations? In this chapter, we will compare one- and two-way nesting in three-dimensional continually-stratified simulations of mountain lee waves and multicell thunderstorms. While this study is not intended to be a comprehensive examination of reflections due to nesting strategy in a stratified system, we can use the examples presented here to determine the sensitivity to the nested grid boundary and to explain some of the behavior using ideas motivated by the shallow water simulations. We will find that while the difference between one-way and two-way nesting is not clear-cut in the trapped-wave simulations, two-way nesting will produce much smaller precipitation errors than does one-way nesting in the multicell simulations.

3.1 Mesoscale model

The model used here is the fully-compressible model used by Piani et al. (2000):

$$\begin{aligned}
\frac{\mathrm{D}\mathbf{u}}{\mathrm{D}t} + c_p\theta\nabla(\pi+\overline{\pi}) &= g\left(\frac{\theta-\overline{\theta}}{\overline{\theta}}\right)\mathbf{k}+\mathbf{D} && (3.1)\\
\frac{\mathrm{D}\theta}{\mathrm{D}t} &= D_\theta + K_\theta && (3.2)\\
\frac{\mathrm{D}\left(\pi+\overline{\pi}\right)}{\mathrm{D}t} &= \frac{R}{c_v}\left(\overline{\pi}+\pi\right)\left(\frac{1}{\overline{\overline{\theta_B}}}\frac{D\theta_B}{Dt} - \nabla\cdot\mathbf{u}\right) && (3.3)
\end{aligned}$$

in which $\mathbf{x} = (x, y, z)$ is the position vector, $\mathbf{u} = (u, v, w)$ the velocity vector,

$$\pi(x,y,z,t) + \overline{\pi}(z) = \left(\frac{p}{p_0}\right)^{R/c_p}$$

the full Exner function (perturbation plus basic state), p the pressure, $p_0 = 1000\,\mathrm{hPa}$, θ the potential temperature with a horizontally-uniform, time-independent basic state $\overline{\theta} = \overline{\theta}\,(z)$, g the acceleration due to gravity, $\mathbf{k}$ the vertical unit vector, $\mathbf{D} = (D_u, D_v, D_w)$ the subgrid scale mixing of momentum (Durran and Klemp, 1983), D_θ the subgrid scale mixing of heat, K_θ the latent heating due to microphysics, R_d the ideal gas constant for dry air,

$$\theta_B = \theta(1 + 0.61q_v)(1 - q_c) \tag{3.4}$$

is the virtual temperature, c_p and c_v the specific heats at constant pressure and volume, respectively. Here, $\frac{D}{Dt} = \frac{\partial}{\partial t} + \mathbf{u} \cdot \nabla$ is the total derivative. Moist processes are included through the use of Kessler warm rain microphysics (Durran and Klemp, 1983): the continuity equation for each water species is

$$\frac{\mathrm{D}q}{\mathrm{D}t} = K_q + D_q \tag{3.5}$$

in which q represents either of the three water species, water vapor q_v, cloud water q_c, or rain water q_r; D_q is the subgrid scale mixing of the species, and K_q the contribution from the microphysics parameterization. No surface fluxes or radiative heating are used in these simulations. Microphysics is disabled in the lee wave simulations, in which $q = 0$ for all three water species, $K_\theta = 0$, and $\theta_B = \theta$.

The discretization uses leapfrog time-differencing with partial time-splitting to handle physically-insignificant acoustic modes (Durran and Klemp, 1983). Spatial discretization is on the Arakawa C-grid. Horizontal momentum and scalar advection are discretized by either second- or fourth-order centered differencing depending on the simulation, although fourth-order differencing will be used unless otherwise mentioned; vertical momentum advection is second-order centered-differencing. Fourth-order artificial dissipation of the form (2.7) is added with $\gamma_4 = 0.1$ to suppress computational noise. At the upper boundary the radiation BC of Klemp and Durran (1983) is used to prevent reflections of vertically-propagating gravity waves. No Coriolis force is applied.

The formulation of the nested-grid boundary conditions in this model, and the updating method in the two-way cases, are the same as for the 1D shallow-water model described in Chapter 2. Simulations using the sponge BC are extended by 5 gridpoints all the way around the nested grid to contain the sponge zone so as to keep the size of the interior solution region the same as for simulations using the interpolation BC.

3.2 Trapped lee waves

3.2.1 Experimental Design

The lee wave simulations used a doubly-periodic coarse grid measuring 720 km by 180 km in the horizontal with a domain depth of 15 km. Several different nested grids were used. The grid which will most often be considered is the “basic” grid, spanning from $x = 51$ to 99 km. Errors are characterized by the differences of the basic grid from a control simulation, which is otherwise identical (including the BC, nesting strategy, and the location of the other boundaries) except the downstream boundary is moved to $x = 201$ km. This method allows us to isolate reflections directly caused by the trapped lee wave’s attempt to exit the basic nested grid.

All of the nested grids span 90 km in the y-direction. An infinitely-long-in-y Witch of Agnesi ridge of height $H = 50$ m and half-width 3 km was placed at $x = 70$ km. Ideally this would create a solution which is uniform in y, but since the nested grid has a finite extent in the y-direction (as in most mesoscale models) and since the nested- and coarse-grid solutions differ in our simulations, we expect disturbances to radiate inward from the north and south boundaries of the nested grid. In our simulations these disturbances are minor compared to the reflections forced by the lee wave at the east and west boundaries of the nested grids, but they do cause some nonstationarity which will be apparent in our solutions and error plots as they propagate across the nested grid. We will not specifically consider these errors in our analysis.

We will find that there are not only errors caused by the reflections from the downstream boundary but also by the errors reflecting again from the upstream boundary. An example of this "secondary reflection", propagating inward from the upstream boundary, can be seen in Fig. 3.1a and (more clearly) in Fig. 3.2a. If we wish to isolate the upstream-propagating "primary reflections" a second pair of grids is used. The first is an extended basic grid, in which the downstream boundary remains at $x = 99$ km but the upstream boundary is moved to $x = -51$ km, so that the primary reflections are unaltered from those in simulations using the basic grid but the secondary reflection does not occur before the end of the simulation. Errors in the extended basic grid simulations—the primary reflections—are deviations from an extended control simulation whose upstream boundary is also moved to $x = -51$ km.

The simulations use coarse-grid horizontal spacings Δx_c, Δy_c of 3 km and nested-grid horizontal spacings Δx_n, Δy_n of 1 km. The timesteps are 15 and 5 s on the coarse and nested grids, respectively, using partial time-splitting with five acoustic timesteps per long timestep. The vertical grid spacing Δz is a uniform 200 m on both grids.

We use the initial condition REF used in the trapped lee wave simulations of Nance and Durran (1998, henceforth ND98). This uses a constant, uniform background westerly flow $U = 10 \text{ m s}^{-1}$, accelerated from rest over the interval $t = -0.5$ to 0 hr, and a two-layer static stability profile

$$N = \begin{cases} N_\ell = 0.01007 \text{ s}^{-1} & 0 \le z \le d \\ N_u = 0.00316 \text{ s}^{-1} & z > d \end{cases} \tag{3.6}$$

where $d = 3$ km is the depth of the lower layer with static stability N_ℓ, and N_u is the static stability in the overlying layer. Here, the static stability is defined as

$$N^2 = \frac{g}{\theta_0}\frac{\partial\overline{\theta}}{\partial z}. \tag{3.7}$$

This profile's approximate Scorer parameter N/U decreases with height sufficiently that wave trapping is expected. Nance and Durran (1997) found for well-resolved

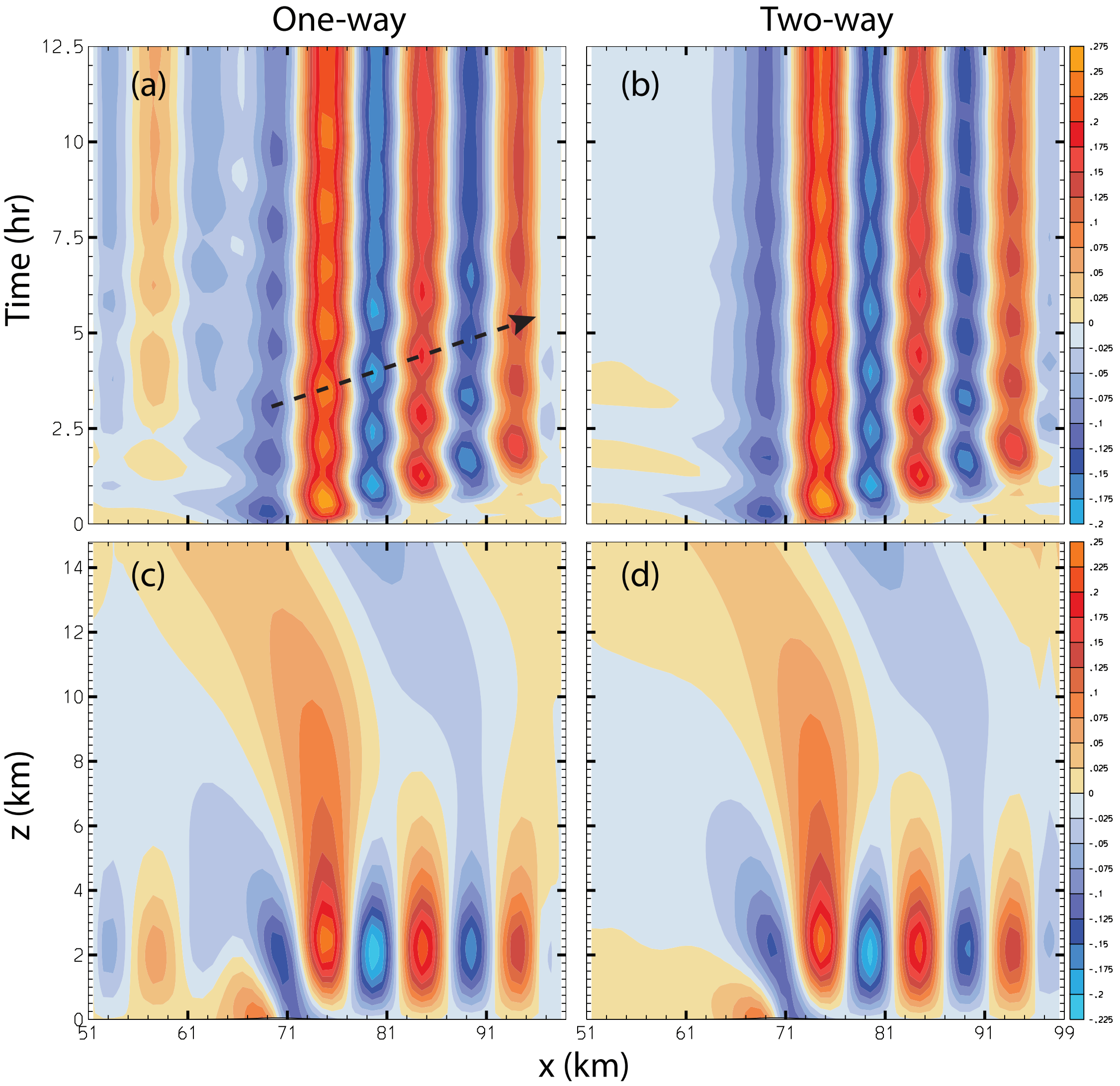

Figure 3.1: Vertical velocity (CI = 0.025 m s^{-1}) for simulations using the interpolation BC. Plots of x vs. t at $z = 3$ km are shown for (a) one-way and (b) two-way nesting; plots of x vs. z at $t = 12.5$ hr are shown for (c) one-way and (d) two-way nesting. Arrow in (a) represents group-velocity vector for the trapped wave. In this and all other lee-wave figures, the mean flow is from left to right, y has been fixed on the east-west centerline of the basic nested grid, and the ridge is at $x = 70$ km.

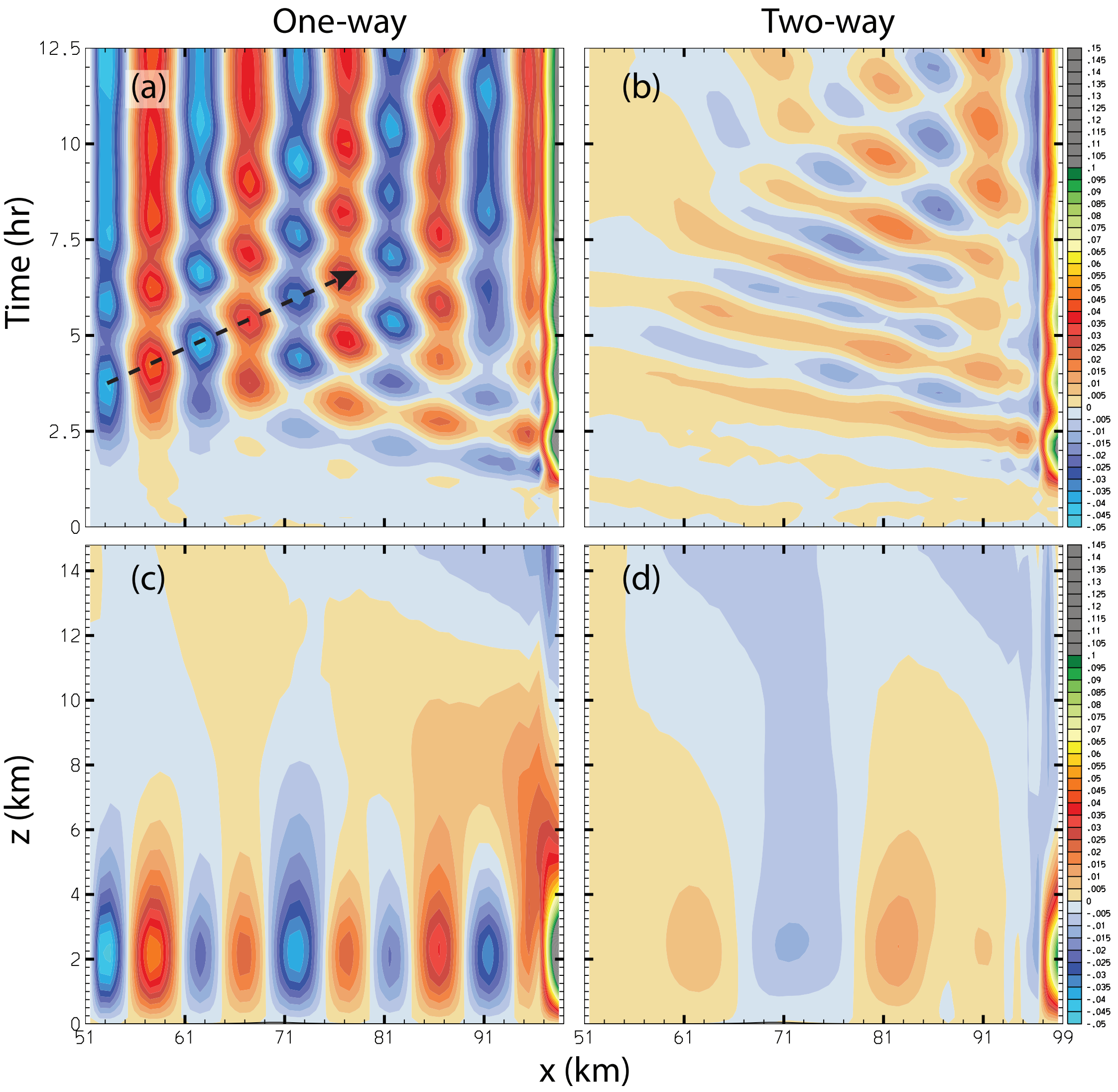

Figure 3.2: As in Fig. 3.1, but for vertical velocity errors (CI = 0.005 m s^{-1}) and that (c,d) show t = 6 hr. Arrow in (a) denotes group-velocity vector for the secondary reflection.

solutions that this profile would create a stationary trapped lee wave of horizontal wavenumber $k = 6.75 \times 10^{-4}\mathrm{m}^{-1}$, corresponding to a wavelength $\lambda = 2\pi/k$ of about 9 km. Note that the coarse grid only uses three gridpoints to represent a wavelength of this trapped wave. The nonlinearity parameter for the lower layer is $N_\ell H/U = 0.05$ so the solution is well described by linear dynamics.

Most of our lee-wave simulations use fourth-order horizontal advection for both momentum and scalars; however, second-order horizontal advection was used in several simulations. When these simulations used the sponge BC, the solution remained stable, but using the interpolation BC caused instability in both one-way and two-way nesting. (We were not able to find the source of this instability.) Thus, only the sponge BC will be used in simulations with second-order advection.

3.2.2 Results

We begin by examining the vertical velocity w on the nested grids of one- and two-way simulations using the interpolation BC and fourth-order horizontal momentum advection (Fig. 3.1). The solutions are broadly similar to those of ND98, as seen in their Figs. 1a and 3a. Both simulations produce a nearly-stationary train of trapped lee waves downstream of the ridge (at $x = 70$ km) with a horizontal wavelength of roughly 9 km and a decaying structure in the vertical above 3 km. Also present is a longer-horizontal-wavelength, vertically-propagating wave which has an intrinsic frequency small enough so it can propagate into the upper layer.

The most apparent difference between the simulations in Fig. 3.1 is a disturbance upstream of the mountain resembling the trapped lee wave in the one-way case (Fig. 3.1ac). This mode does not appear among the primary reflections in the extended-grid simulations (Fig. 3.3) and is the aforementioned "secondary reflection". The structure of the secondary reflection is clearly seen in the error plot of Fig. 3.2a, which shows a quasi-steady disturbance propagating from the upstream boundary with an amplitude of roughly 20% of that of the physical lee wave. The secondary reflection is much weaker in the two-way case (Fig. 3.2b) and is not the major source of error in two-way nesting. We will demonstrate the source of this reflection below.

We can check the group velocity of the incident lee wave and of the secondary reflection with that expected for a Boussinesq gravity wave in a uniform N and U fluid (a valid approximation to our two-layer simulations, as each layer acts as a single fluid with forcing applied to the bottom and/or top). The horizontal phase speed in the lower layer is

$$c = U - \frac{N_\ell}{\mathcal{K}}, \tag{3.8}$$

and the horizontal group velocity is

$$c_{gx} = U - \frac{N_\ell \ell^2}{\mathcal{K}^3} \tag{3.9}$$

where $\mathcal{K} = \sqrt{k^2 + \ell^2}$, and (k, ℓ) is the wavenumber vector. The incident trapped wave (Fig. 3.1c) and the secondary reflection (Fig. 3.2c) have a horizontal wavelength of about 9 km. Since both the trapped wave and the secondary reflection are stationary, the vertical wavelength $\lambda_z = 2\pi/\ell$ must yield $c = 0$. Solving (3.8) for ℓ finds that the vertical wavelength must be about 8.5 km, for which (3.9) yields 4.8 m s^{-1}. Figs. 3.1a and Fig. 3.2a show that the downstream propagating modes' group velocity is about 3.1 m s^{-1}. The discrepancy between the theoretical values and those seen in the simulations[1] may be due to numerical dispersion errors artificially decreasing the group velocity; a simulation with Δx_n decreased to 500 m produced a group velocity of about 3.5 m s^{-1}.

Both the one-way and two-way simulations show substantial primary reflections (Fig. 3.3), most of which are larger in two-way nesting; however the primary reflections in both simulations are smaller than the one-way simulation's secondary reflection. (Comparing Figs. 3.2b and 3.3b reveals the secondary reflection present in the two-way simulation, which is of lower amplitude than the two-way simulation's primary

---

[1] Fig. 3a in ND98 shows a stationary wave with a similar group velocity. Nance and Durran (1997) derive a more complicated formula (their equation 9) for the group velocity of a trapped wave in a two-layer flow, which gives the same value for our trapped wave as does (3.9).

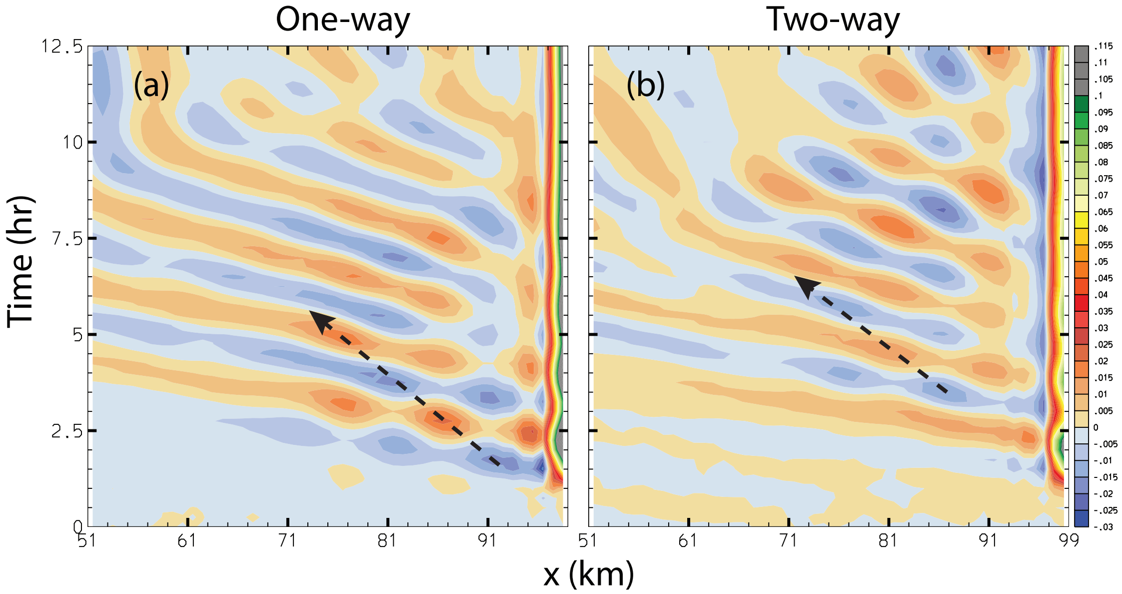

Figure 3.3: As in Fig. 3.2ab, but for vertical velocity errors in the extended simulation, isolating the primary reflections. Arrows denote group-velocity vectors for the primary reflections.

reflections and of much lower amplitude than the secondary reflection in the one-way case.) Unlike the stationary secondary reflection, the primary reflections are non-stationary, show upstream propagation and have a longer horizontal wavelength of about 20 km. In the vertical, a quarter-wavelength of the wave is seen to span the 3-km-deep lower layer of the atmosphere (cf. Fig. 3.2d), and we estimate the vertical wavelength to be about 12 km. The resulting phase speed from (3.8) is -6.5 m s^{-1}, and the group velocity from (3.9) is -2.1 m s^{-1}. The primary reflections in Fig. 3.3 demonstrate phase speeds of about -6.1 and -5.9 m s^{-1} for one-way and two-way nesting, respectively, and group velocities of -1.2 and -1.4 m s^{-1}.

What causes the primary reflections? Recall from the 1D shallow-water model in Chapter 2 that errors in one-way nesting are due to a mismatch between the coarse- and nested-grid solutions, while errors in two-way nesting are primarily related to the change in group velocities between the two grids, which in turn is directly related to how well-resolved the disturbance is between the two grids. Reflections are expected in the one-way case from the severe mismatch between the coarse and nested grids, since the coarse-grid solution does not exhibit a strong trapped lee wave and in fact has very little vertical velocity at the boundary of the nested grid (Fig. 3.4a). (The zero value at the downstream BC is clearly seen in Fig. 3.1a.)

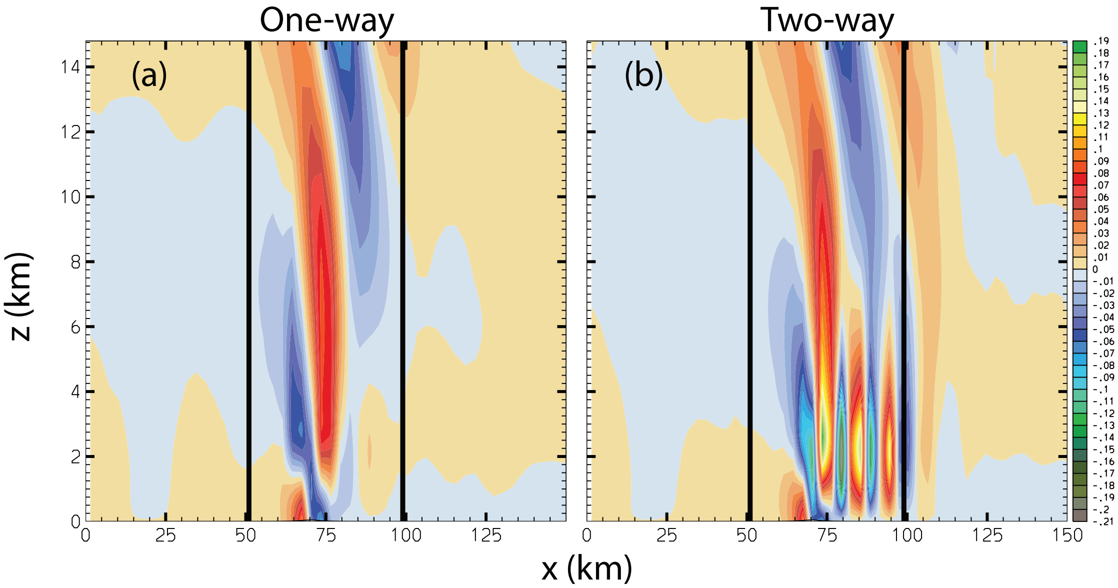

Figure 3.4: Coarse-grid plot of w (CI $= 0.01$ m s^{-1}) in simulations with the interpolation BC at $t = 6$ hr for (a) one-way and (b) two-way nesting. Boundaries of the nested grid are given as vertical bars.

In the two-way case, Fig. 3.4b shows that very little of the amplitude of the trapped wave is seen beyond the nested grid's boundary, implying that either the group velocity of the trapped wave is greatly reduced on the coarse grid or that the trapped wave is unable to propagate on the coarse grid. Further, the lee wave "untraps" on the coarse grid and becomes vertically propagating, which is more easily seen in a simulation with a weaker damping of $\gamma_4 = 0.02$ (Fig. 3.5); the usual dissipation of

$\gamma_4 = 0.1$ quickly damps the vertically propagating wave produced as the lee wave propagates onto the coarse grid. In the more weakly-damped case the trapped wave is still unable to propagate onto the coarse grid, indicating that the lack of a trapped wave on the coarse grid in Fig. 3.4 is not due to stronger damping in those simulations. The large difference in group velocities and even the basic behavior of the lee wave between the two grids implies that we should expect strong reflection from the downstream boundary in the two-way case.

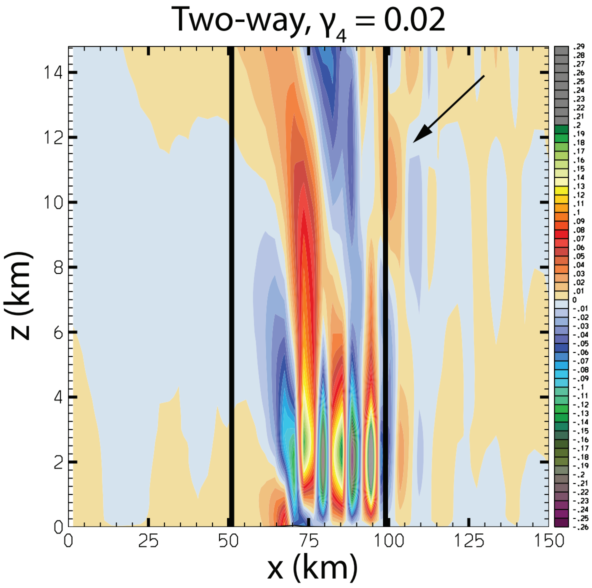

Figure 3.5: As in Fig. 3.4b, but for a two-way nested simulation with γ_4 reduced to 0.02. The vertically-propagating disturbance is indicated by the callout.

.

The secondary reflection is the primary reflection reflecting again off of the upstream boundary. In the one-way case, the primary reflection (Fig. 3.6b) reaches the upstream boundary just after $t = 2.5$ hr, coinciding with the appearance of the secondary reflection (Fig. 3.2a). Here, we have shown the surface pressure response of the primary reflection, which more clearly shows its progress towards the upstream boundary than does the w field. The primary reflection also reaches the upstream boundary in the two-way simulation (Fig. 3.7b), but much less reflection of this mode occurs in the two-way case, which is apparent as the relatively weak secondary reflection in Fig. 3.2b.

Why does the primary reflection cause a larger reflection at the upstream boundary in the one-way case than the two-way case? Comparing the coarse-grid surface p (Fig. 3.6a) to that of the primary reflection on the nested grid (Fig. 3.6b) shows that the solutions on the two grids are very different, causing a mismatch at the nested-grid boundary and creating the secondary reflection.

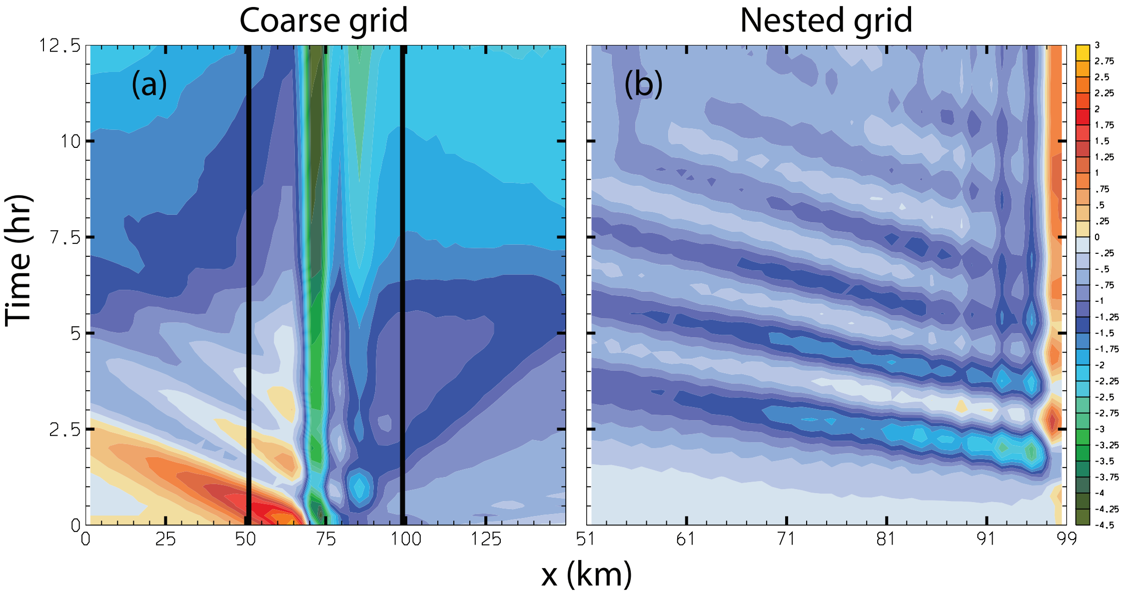

Figure 3.6: Surface p (CI = 0.25 Pa) in a one-way nested simulation using the interpolation BC. (a) Coarse-grid (black bars represent boundaries of nested grid); (b) Nested grid errors on the extended grid, to isolate the primary reflection.

Alternately, since the primary reflection is well-resolved on both grids, the difference in computational group velocities is expected to be small between the two grids, and in two-way nesting this mode should propagate onto the coarse grid with less reflection than in the one-way case. Indeed, Fig. 3.7b (depicting the full error, including any secondary reflections) shows that the primary reflection is able to propagate onto the coarse grid largely unimpeded in the two-way nested simulation without creating a substantial secondary reflection.

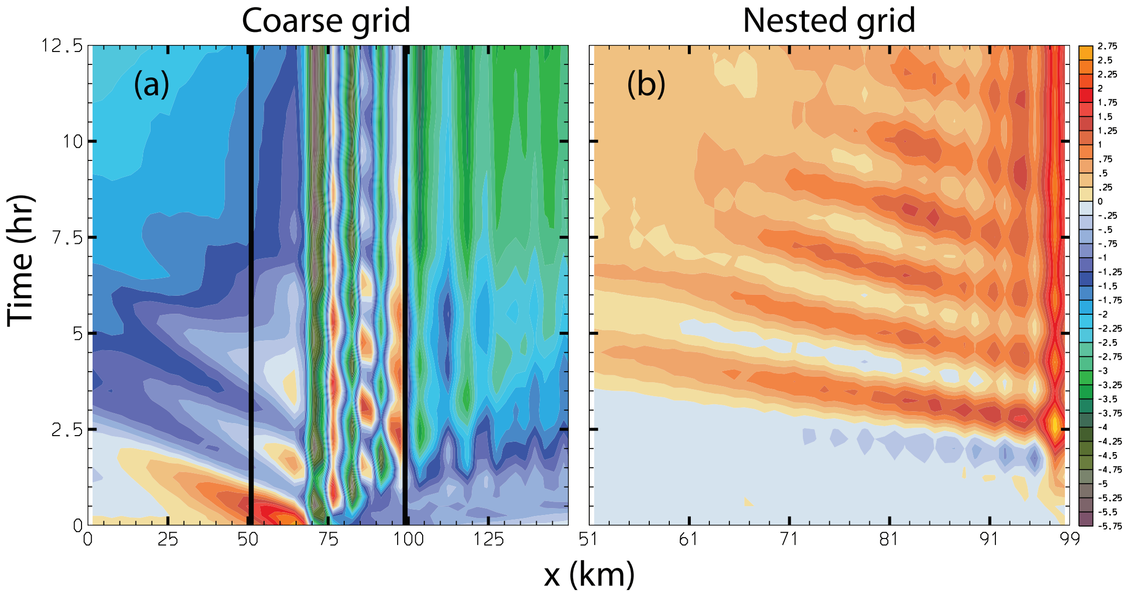

Figure 3.7: As in Fig. 3.6, but for two-way nesting, and that (b) shows the full p error field.

Using the sponge BC should reduce the reflections in both one-way and two-way nesting. In one-way nesting this is certainly true (Fig. 3.8ac) as the secondary reflection is substantially reduced in amplitude and the primary reflections are slightly smaller than for the interpolation BC (Figs. 3.2a, 3.3a). In the two-way simulation (Fig. 3.8bd), the primary reflections are actually larger than when the interpolation BC is used (Fig. 3.3b). Why would reflections become more severe in two-way nesting when the sponge BC is used? Recall that in two-way shallow-water simulations, short wavelength nested-grid disturbances propagated onto the coarse grid as $2\Delta x_c$ or evanescent modes, creating a coarse-grid solution inconsistent with that on the nested grid and interfering with the sponge BC's ability to damp outgoing waves. I tentatively claim that a similar inconsistency between the coarse- and nested-grid solutions is occurring in these trapped-wave simulations, which again degrades the sponge BC's effectiveness in damping outgoing waves. In this 3D simulation, the inconsistency is between the trapped lee wave on the nested grid and the untrapped wave on the coarse grid.

Unlike in the shallow-water model, applying the filtered sponge BC does little to change the amplitude of the reflections. In this case the coarse-grid solution being relaxed to is not dominated by $2\Delta x_c$ waves and so filtering the coarse-grid data was found to have little effect.

Using second-order horizontal momentum and scalar advection reduces the errors in both the one-way and two-way cases (Fig. 3.10), although the errors are again larger in two-way nesting than in one-way nesting. The secondary reflection is absent in both simulations. In these simulations, the incident trapped wave is lower-amplitude (Fig. 3.11) than in the fourth-order simulations (Fig. 3.1d), and so we expect the reflections to be smaller.

3.3 Multicell thunderstorm

3.3.1 Experimental Design

The multicell simulations use fourth-order horizontal momentum advection, and scalar advection (of potential temperature and microphysical species) is performed by the flux-limited finite-volume advection scheme of LeVeque (1996). No partial time-splitting is used.

The model is initialized using a thermal structure from Weisman and Klemp (1982) with a 14 g kg^{-1} water vapor mixing ratio uniform throughout a 1000 m-deep mixed layer; a surface and tropopause temperature of 300 K and 213 K, respectively; a tropopause potential temperature of 343 K; and a tropopause height of 12 km. The

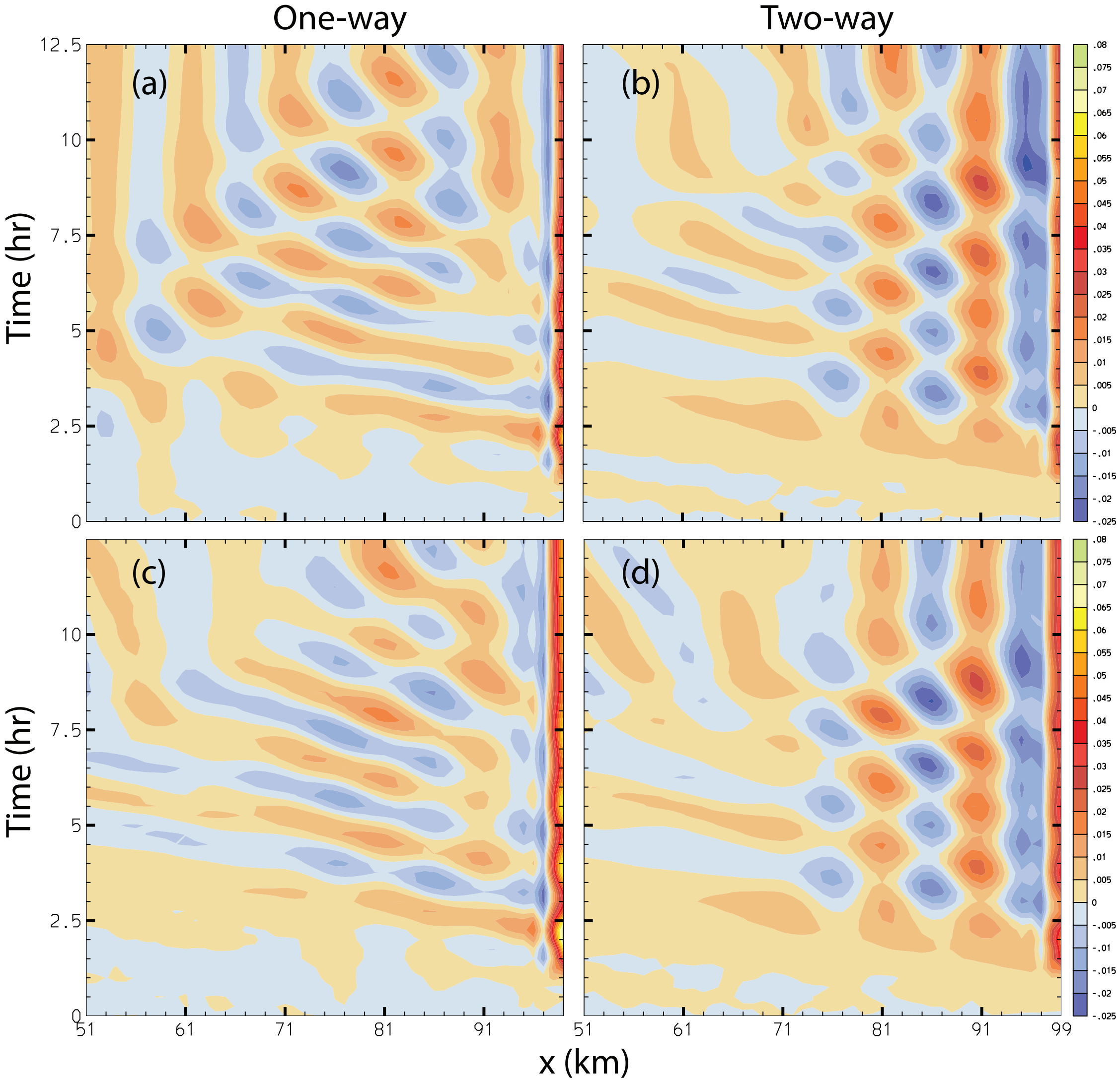

Figure 3.8: (a) and (b): As in Fig. 3.2a,b, but for the sponge BC. (c) and (d): As in (a) and (b) but for errors on an extended grid, isolating the primary reflections.

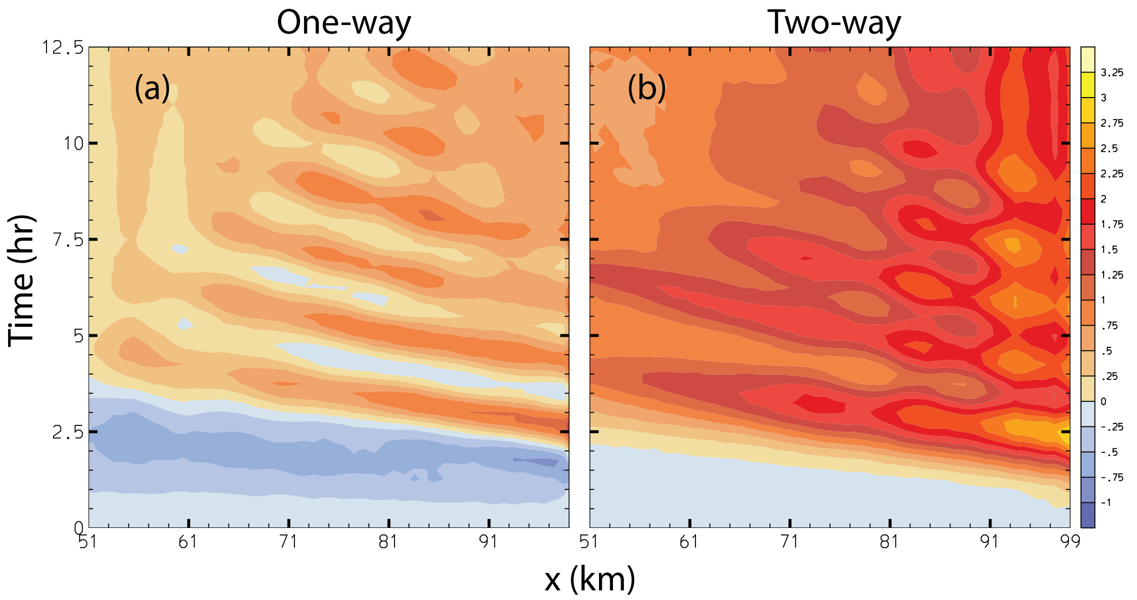

Figure 3.9: Surface p (CI = 0.25 Pa) error in a simulation using the sponge BC. (a) One-way nesting; (b) two-way nesting.

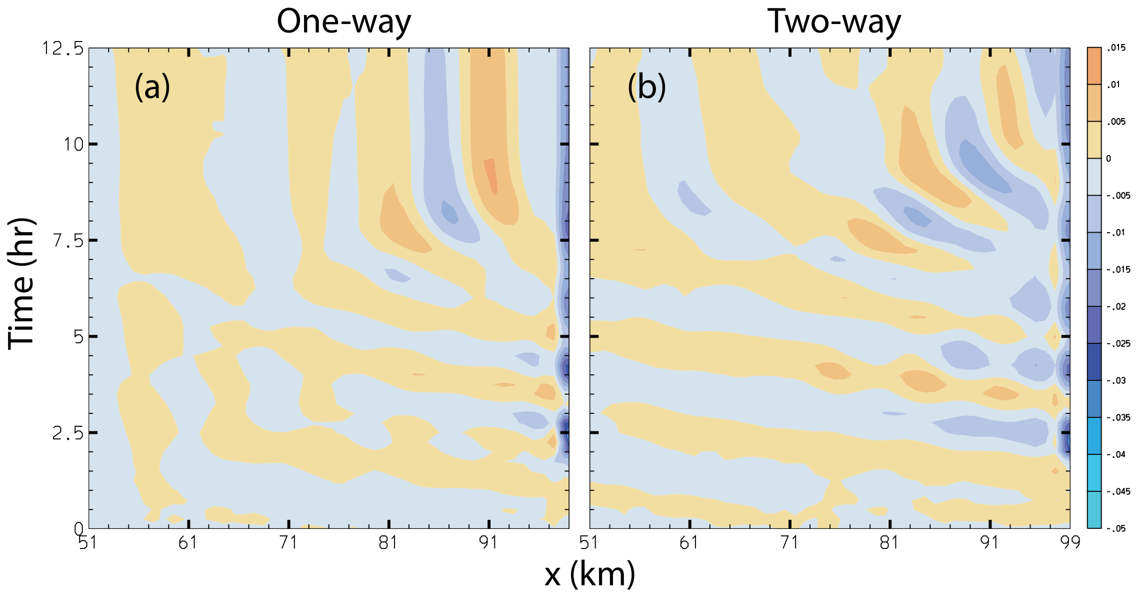

Figure 3.10: As in Fig. 3.2ab, but for second-order advection and the sponge BC.

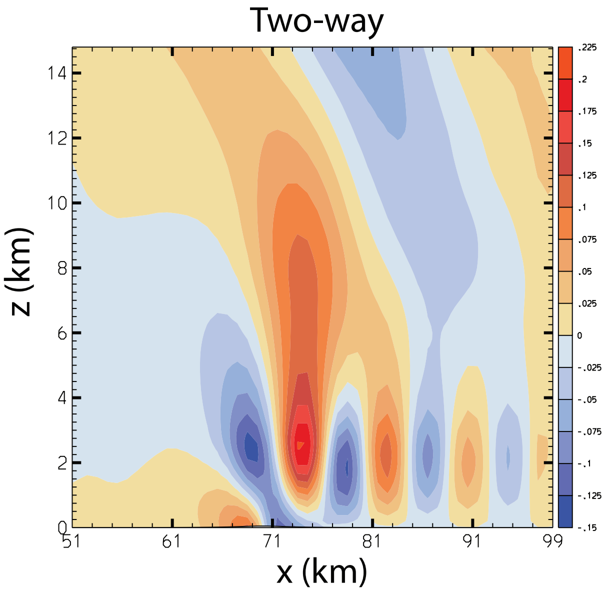

Figure 3.11: As in Fig. 3.1d, but for second-order advection and the sponge BC.

winds are 5 m s^{-1} from the west at the surface, and increase linearly with height to 17 m s^{-1} at 2000 m, and are constant above that height; there is no directional shear. This profile (Fig. 3.12) yields a bulk Richardson number of about 150, well within the range for multicell thunderstorms (Weisman and Klemp, 1982).

The coarse grid's dimensions are 498 km by 606 km (Fig. 3.13), with a horizontal grid spacing Δx_c of 3 km. The domain extends to 14.85 km above the surface with a constant vertical grid spacing of 150 m. The coarse grid uses a timestep of 3 s and model runs were integrated to 4 hr. The coarse grid uses an outflow BC with an outflow gravity wave speed of 30 m s^{-1}, as suggested by Fovell et al. (1992). The convection was initiated by a warm bubble of radius 20 km, 5 K warmer than its environment, centered at the surface and at x = 150 km, y = 300 km. The nested grids used a timestep of 1 s and a horizontal grid spacing Δx_n of 1 km. The vertical structure was identical on both grids.

Several different nested-grid domains were used in these experiments: a control case with a nested grid measuring 252 km by 360 km, and two smaller grids, each 158 km in both horizontal directions. The primary small grid is positioned so that the warm bubble is centered within the grid in the north-south direction; a second, "shifted" small grid is the same as the primary small grid but shifted southward 38 km. The solution within the small-grid subdomain of the control case was not sensitive to the nested grid formulation, since neither the storms nor any convectively-generated disturbances reach the control grid's boundaries in time to affect the small-grid domain. In the discussion below, the control simulation is considered to be "truth", and we characterize deviations from the control in the other simulations as "errors". The nested grid BCs are the same as those in the lee wave and shallow-water simulations.

3.3.2 Results

All of the simulations depict a qualitatively similar solution on the nested grid: a multicell thunderstorm is initiated by the warm bubble, and gradually evolves into multiple individual cells while propagating eastward, so that the storm comprises several cells by the time it reaches the eastern boundary of the small nest, all leaning upshear in the mature phase of their evolution. Plots of precipitation accumulated over the entire four-hour integration time of the control simulation (Fig. 3.14a) show the path of the storm and the individual cells, including where new cells form.

Errors arising from using the smaller nested grid are apparent in the one-way simulation depicted in Fig. 3.14b, in which the interpolation BC is used. The most obvious errors are those at the two gridpoints closest to the eastern boundary, where the accumulated precipitation is nearly double that in the control simulation. These errors are attributed to a spurious increase in the updraft strength as the storm attempts to exit the nested grid, and the mass convergence of rainwater unable to pass through the nested-grid boundary. Similar errors are seen in all of the small nest cases depicted in Fig. 3.15, but none of them are as large as in the one-way

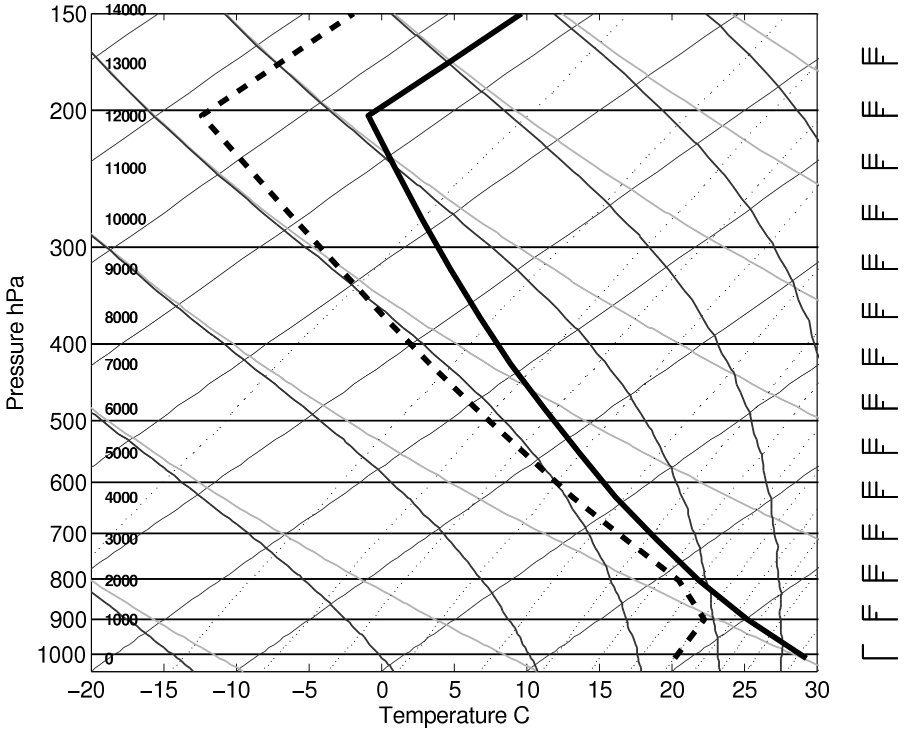

Figure 3.12: Skew-T plot of basic-state sounding for multicell simulations. Heavy solid line is temperature of the basic state (contours of which are heavy black lines slanting upward to the right), heavy dashed line is the mixing ratio (contours of which are dashed lines). Bold numbers on the left-hand side are heights (in meters) of points in the profile.

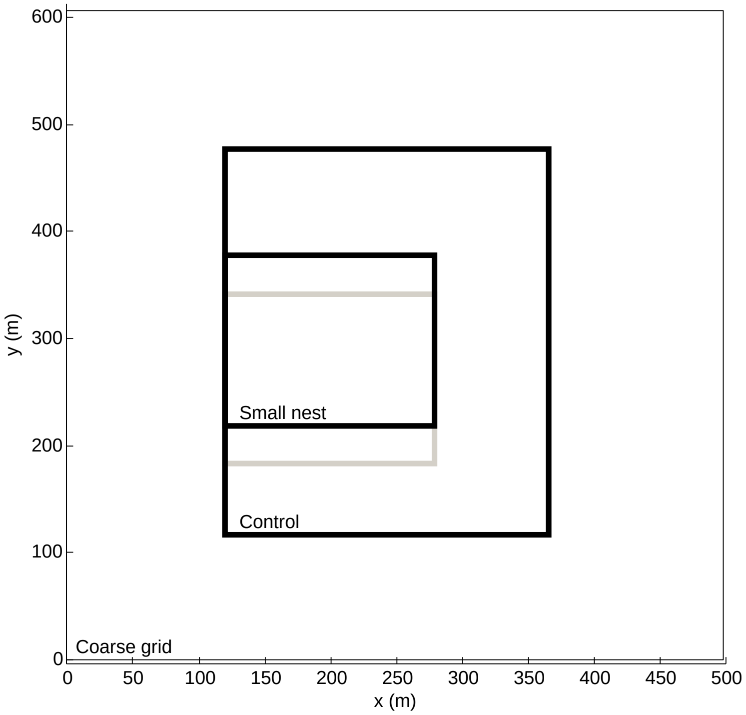

Figure 3.13: Schematic of domains used for multicell cases. The “shifted” small grid is outlined in gray. The control nest includes the entirety of both small nests.

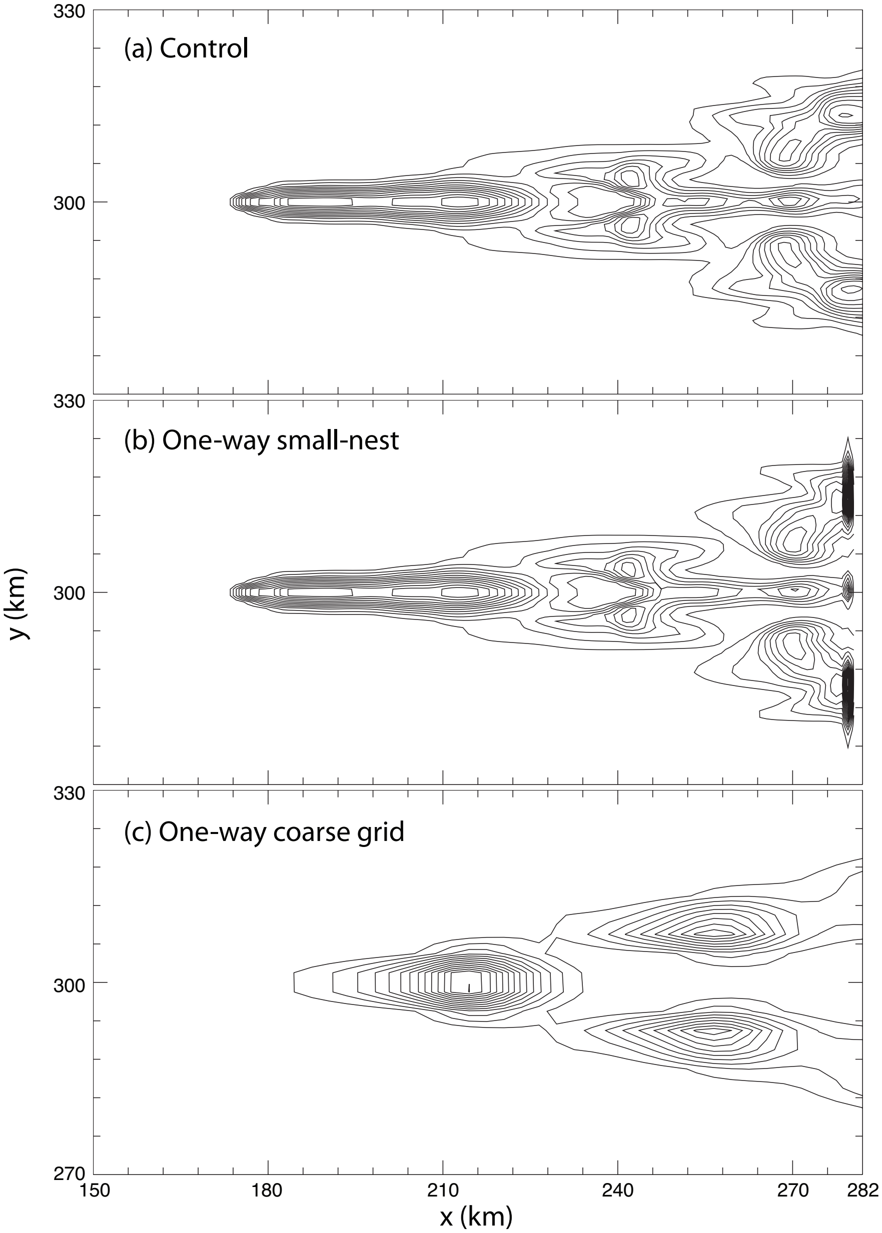

Figure 3.14: Nested-grid accumulated precipitation for (a) the control multicell simulation; (b) the one-way small-nest multicell simulation using the interpolation BC. (c) Accumulated precipitation on the coarse grid in a one-way nested simulation. Contour interval is 0.2 cm. In this and in all precipitation plots only a subset of the small-nest simulation is shown, and (unless otherwise specified) only precipitation on the nested grid is shown.

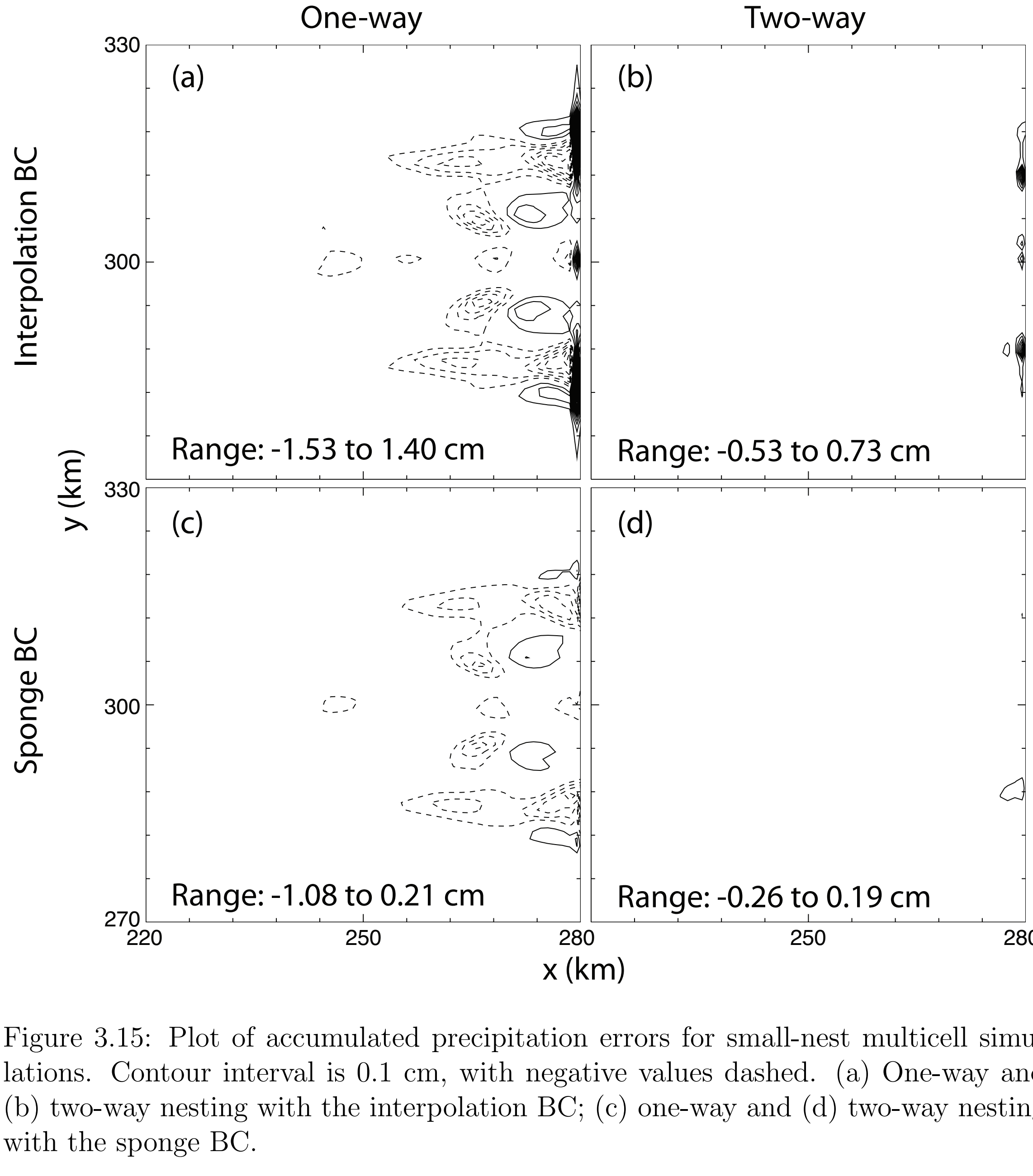

Figure 3.15: Plot of accumulated precipitation errors for small-nest multicell simulations. Contour interval is 0.1 cm, with negative values dashed. (a) One-way and (b) two-way nesting with the interpolation BC; (c) one-way and (d) two-way nesting with the sponge BC.

case using the interpolation BC. In addition, more modest errors extending nearly 30 km ($30\Delta x_n$) from the nested grid's eastern boundary can be seen in the one-way cases (Fig. 3.14b, Fig. 3.15a,c). These occur before the updrafts reach the boundary, and are attributed to a disturbance such as a convectively-generated gravity wave reflecting off of the nested grid boundary and interfering with the storm. Reflection of gravity waves is clearly seen in Fig. 3.16a where the annular structure of the gravity wave (seen undisturbed in the control simulation in Fig. 3.16b) is altered along the outflow (right-hand) boundary. Reflection can also be seen from the other boundaries of the one-way nest. The vertical structure of the gravity wave (Fig. 3.16d) also differs from the control simulation (Fig. 3.16e): although the crests of the outgoing wave are apparent, the amplitude of the wave crests are different, and the wave is severely distorted against the boundary.

The errors are overall much smaller when using two-way nesting. Errors are apparent at the boundary when using the interpolation BC (Fig. 3.15b), but these are smaller and less widespread than when using one-way nesting (Fig. 3.15a). Further, no significant errors are seen in the interior when two-way nesting is used, and little reflection or distortion of the gravity wave is seen (Fig. 3.16cf).

Applying the sponge BC cuts the magnitude of the errors in the one-way case (Fig. 3.15c) by about half in the interior and greatly reduces the errors at the boundary when the sponge BC is used compared to the interpolation BC. These errors are still worse than those in the two-way case (Fig. 3.15d) which likewise has a large reduction in the errors at the boundary and again no significant errors in the interior. Applying the filtered sponge BC has no appreciable effect on the errors for either one-way or two-way nesting.

Our experience with the 1D model lead us to believe that the errors in the one-way case would be caused by mismatched solutions between the two grids. Examining the coarse grid (Fig. 3.17a) at $t = 2.5$ hr reveals a solution very different from that on the nested grid (Fig. 3.17b). While the nested grid has two strong cells about

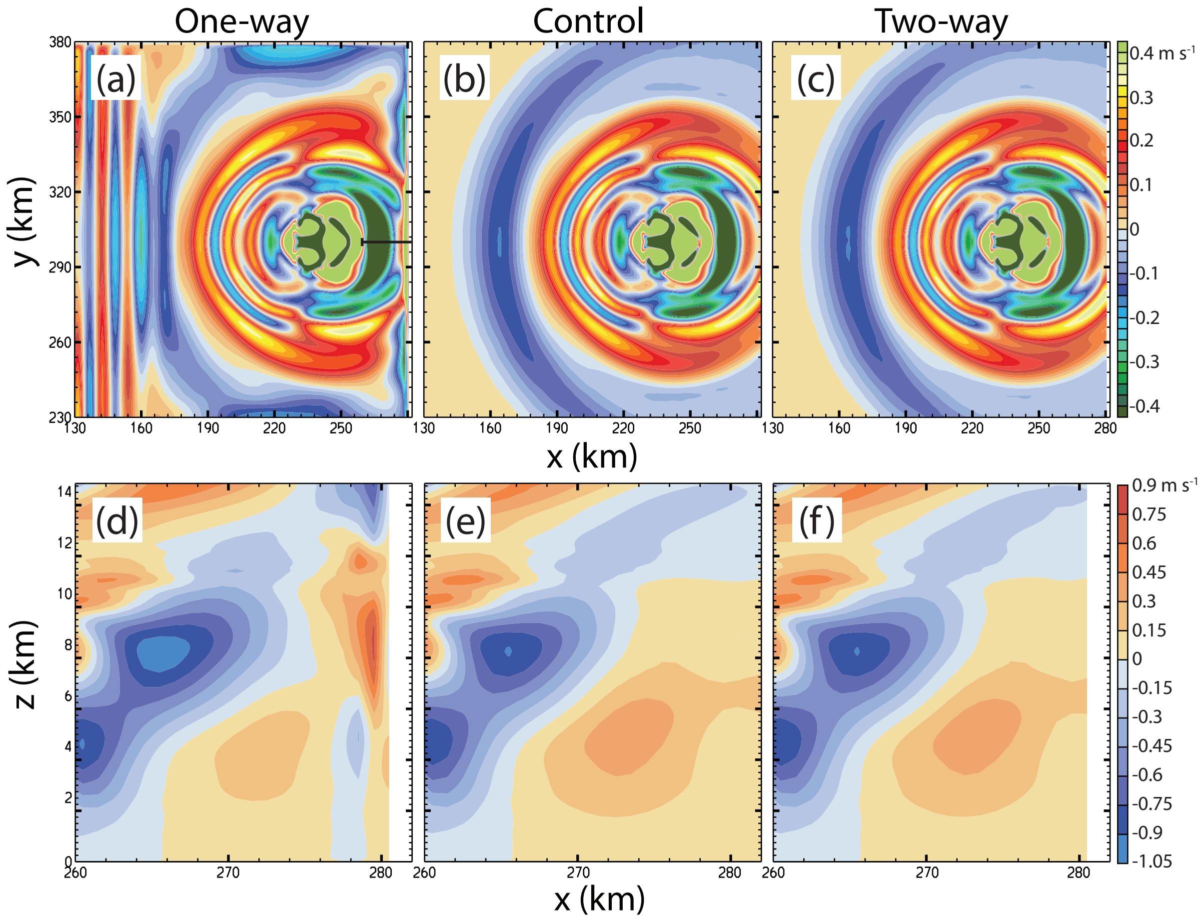

Figure 3.16: Vertical velocity at $z = 9$ km and $t = 120$ min, contour interval 0.025 m s^{-1} (contours beyond ±0.4 m s^{-1} not plotted) in multicell simulations: (a) one-way small-nest simulation; (b) control simulation; (c) two-way small-nest simulation. Vertical velocity along an east-west cross section at $y = 300$ km (denoted by horizontal line in (a)) at $t = 120$ min, contour interval 0.15 m s^{-1}: (d) one-way small-nest simulation; (e) control simulation; (f) two-way small-nest simulation. All simulations use the interpolation BC.

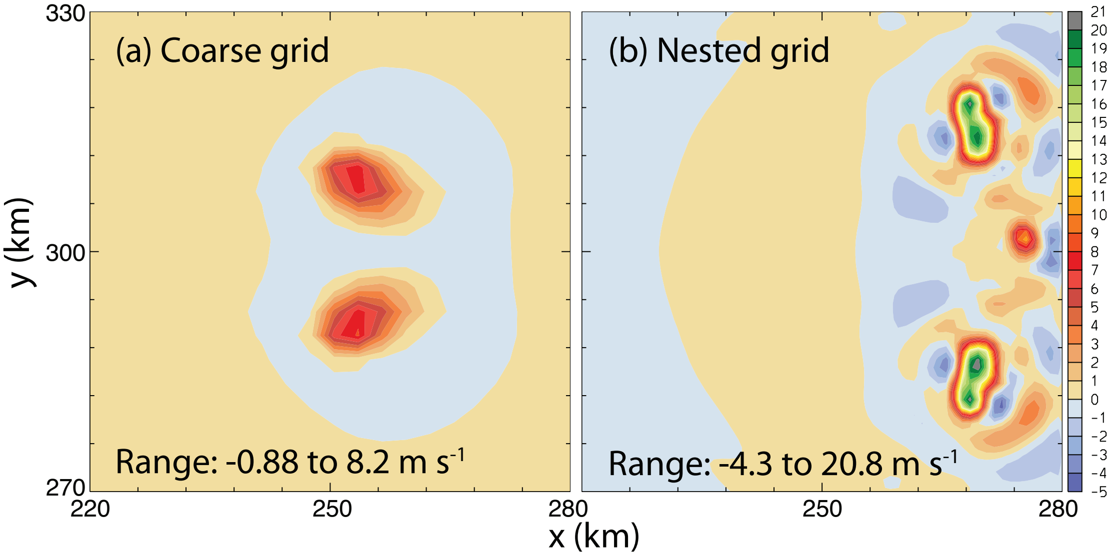

Figure 3.17: Vertical velocity at z = 6 km and t = 2.5 hr in the one-way nested multicell simulation using the small nest with the interpolation BC. (a) Coarse grid; (b) nested grid.

10 km from the nested grid boundary, the coarse grid has two weaker, more diffuse cells which are still nearly 30 km away from the nested grid boundary. Comparing the accumulated precipitation on the coarse grid (Fig. 3.14c) to that on the nested grid (Fig. 3.14b) reveals that the evolution of the storm is very different on the two grids: the nested grid cells are still active as they cross the nest's boundary, while the coarse-grid cells appear to be dying out as they exit the nested grid's domain. The coarse-grid storm also is seen to propagate more slowly, and develop a weaker updraft and cold pool than the nested-grid storm. The two solutions will not match at the boundary, and reflection will occur. The differently-evolving storms also cause different convectively-generated gravity waves: the phase (Fig. 3.18a) and amplitude (Fig. 3.18b) of the coarse-grid gravity wave are both very different from those on the nested grid (Fig. 3.16), and the resulting mismatch causes the reflections seen so clearly in the one-way simulations (Fig. 3.16ad).

The sensitivity of organized convection to model grid spacing is well known. In particular Weisman et al. (1997) found that a simulated quasi-three-dimensional squall line would evolve more slowly and have a weaker updraft as the grid spacing increased. While they found that simulations with grid spacing of 4 km or less were able to broadly reproduce the structure and evolution of a squall line seen in a simulation using a 1 km grid spacing, the exact timing and speed of the storm's evolution as well as its strength could still greatly differ between the 1- and 4-km simulations (cf. their Fig. 17).

Meanwhile, two-way nesting does not suffer from errors in mismatches since the nested- and coarse-grid solutions are held together, and so errors can only occur as the storm attempts to exit the nested grid. The convectively-generated gravity waves are only slightly distorted at the boundary even when using the interpolation BC (Fig. 3.16cf).

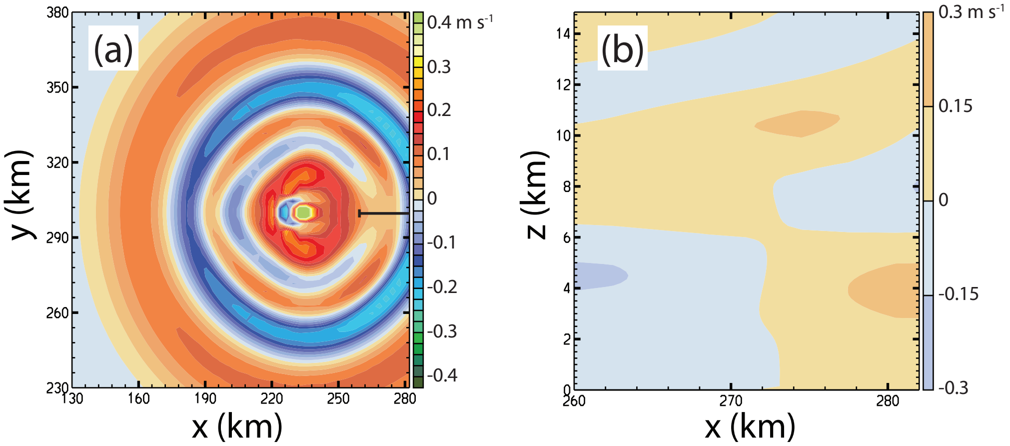

Figure 3.18: As in (a) Fig. 3.16a and (b) Fig. 3.16d for the coarse grid of a one-way small-nest multicell simulation.

How important is the reflected gravity wave in causing errors in the one-way simulations? To answer this question, simulations using the shifted small nest (outlined

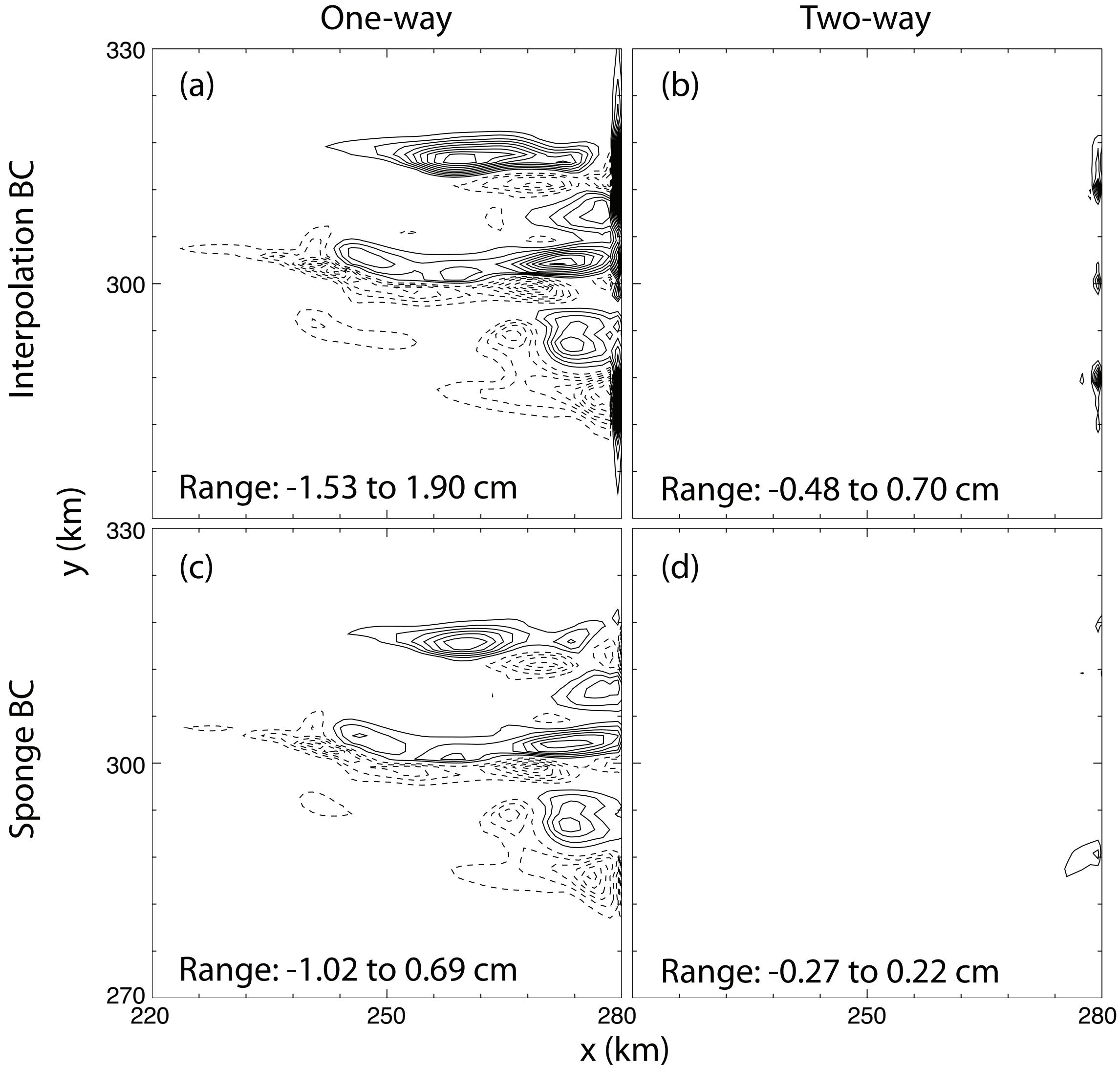

Figure 3.19: As in Fig. 3.15 but for the shifted small-nest simulations.

in gray in Fig. 3.13) were performed. The shifted small nest's northern boundary is close enough to allow the reflected gravity waves to interact with the storm well before it reaches the eastern boundary of the nested grid. Nevertheless, at all times the northernmost cell remains at least 20 km from the location of the northern boundary.

The precipitation errors in the shifted small-nest simulations are seen in Fig. 3.19. In the one-way simulations (Fig. 3.19ac) not only are the errors larger than in the one-way simulations using the original small nest (Fig. 3.15ac) but the extent of the errors has broadened: errors now are seen more than 40 km ($40\Delta x_n$) from any nested grid boundary. Reflection of the convectively-generated gravity waves from the northern boundary is apparent (Fig. 3.20a) as again the waves are disrupted (compare the control solution in Fig. 3.20b). Vertical cross-sections comparing the one-way and control simulations (Fig. 3.20d and e, respectively) show that the vertical structure has also been altered.

The reflected gravity waves have also triggered a new convective cell to the north of the others which is not evident in the previous one-way simulations. Using the sponge BC (Fig. 3.19c) reduces but does not eliminate the errors caused from shifting the nested grid.

Once again, two-way nesting (Fig. 3.19bd) yields much smaller errors than one-way nesting, using either BC. These errors differ little from those in the original small-nest simulations with two-way nesting (Fig. 3.15bd) and the gravity waves (Fig. 3.20cf) are only weakly distorted at the boundary.

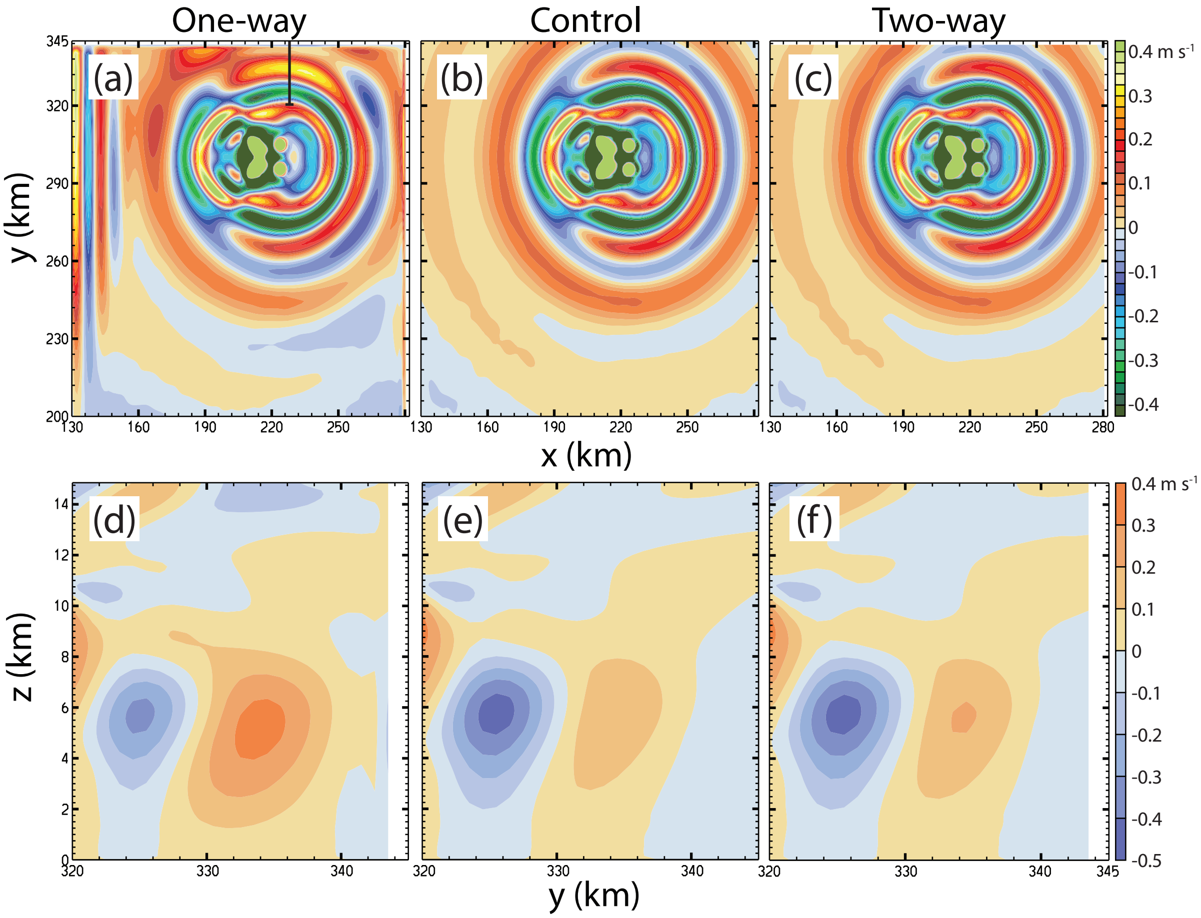

Figure 3.20: Vertical velocity at $z = 6$ km and $t = 95$ min, contour interval 0.025 m s^{-1} (contours beyond ± 0.4 m s^{-1} not plotted) in (a) one-way, (b) control, and (c) two-way shifted small-nest multicell simulations. Vertical velocity in a north-south cross-section at $x = 230$ km (denoted by vertical line in (a)) and $t = 95$ min, contour interval 0.1 m s^{-1} in (d) one-way, (e) control, and (f) two-way shifted small-nest multicell simulations.

Chapter 4

INFLUENCE OF TWO-WAY NESTING ON THE COARSE GRID

One drawback to two-way nesting is that it alters the coarse-grid solution in a manner that can be cosmetically unappealing. This can be illustrated in a simple case where a sinusoidal scalar field is advected in a uniform 5 m s^{-1} flow parallel to the x-coordinate. The initial tracer field is

$$\phi(x, y, 0) = \cos[\pi x/(12\Delta x_n)],$$

which is a monochromatic wave with phase lines parallel to the y-axis and a wavelength of $24\Delta x_n$. The coarse mesh is a doubly-periodic 384-km square with 6-km grid spacing; the line $x = 0$ coincides with the "west" boundary of the domain. The fine mesh is an 184-km-square with 2-km grid spacing. The nested grid uses the interpolation BC. The grids have timesteps of 9 and 3 s, respectively. Since there is no north-south velocity, the numerical scheme reduces to the second-order centered difference method given by (2.6).

The coarse-grid solution in a one-way nested simulation, shown in Fig. 4.1a, remains a simple monochromatic wave as it translates across the mesh. That is not the case for two-way nesting, as shown in Fig. 4.1b. Since the wave is better-resolved on the nested grid, the solution on that grid propagates closer to the correct phase speed, and when the coarse mesh region overlying the fine mesh is updated, it inherits the phase of the more accurate solution on the nested mesh and winds up out of phase with the wave on the surrounding coarse grid. Using the sponge BC instead of interpolation does not reduce the mismatch, since the sponge zone is not used in updating the coarse grid.

The distortion of the coarse-grid solution at the edge of the two-way nest does not necessarily mean that such nesting increases objective measures of the error in the coarse-grid solution. On the contrary, the solution on the coarse grid may be more accurate, because the higher-resolution nested-grid solution is allowed to correct part of the coarse grid solution. As an example, consider the amplitude-normalized root-mean-square error (RMSE), given by:

$$\frac{1}{\phi_0}\sqrt{\frac{\Sigma_N\left(\phi-\phi_E\right)^2}{N-1}}$$

where $\phi_E(x,y,t)=\phi(x-Ut,y,0)$ is the exact solution of the advection equation, ϕ_0 is the amplitude of the IC, and N is the total number of gridpoints in the domain. At the time shown in Fig. 4.1, the RMSE in the one-way case is 1.22, but in the two-way case it is 1.06. In our test case, the difference in RMSE is a function of time. At other times, the difference in RMSE between the two cases is not as large, and at much later times the RMSE of the two-way case becomes larger than that of the one-way case because the accumulated phase speed errors begin to bring the coarse grid solution back in phase with the true solution. Nevertheless, this example serves to demonstrate that the distorted coarse-grid solution generated by two-way nesting is not necessarily less accurate than the undistorted result obtained with one-way nesting.

Modelers who wish to use two-way nesting for its greater accuracy on the nested grid but also wish to have an undisturbed coarse-grid solution are advised to simply perform a second coarse-grid simulation without the nested grid. The increased computational expense of an additional coarse grid run is typically modest. For example, the current (as of 26 May 2009) formulation for the triply-nested WRF simulations run at the University of Washington has nearly four times as many gridpoints on its most deeply nested grid as does the next-finest level of nesting. Since the timestep on the finest grid is one-third of that on the next-finest, the time required to re-run the simulation with only the next-finest grid would only be about one-twelveth that required to run the simulation with the finest nest.

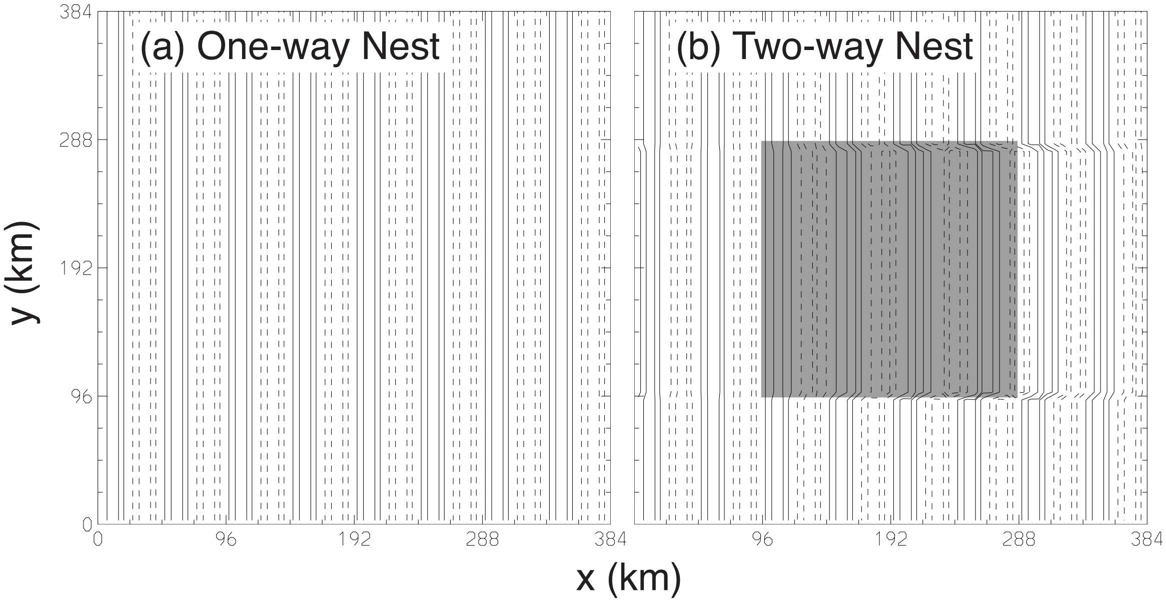

Figure 4.1: Coarse grid solution of the scalar advection equation of a unit-amplitude monochromatic $18\Delta x_n$ wave in a passive tracer field, shown at $t = 9$ h using (a) one-way and (b) two-way nesting. Contour interval is 0.4, negative contours dashed. Shaded box in (b) represents position of nested grid.

Chapter 5

CONCLUSION

Does either one-way or two-way nesting cause less error in a nested-grid simulation? We have used both idealized and more realistic numerical models to answer this question. A one-dimensional shallow water model has been used which permits a simple error analysis and a simple estimate of and explanation for the reflections occurring when using either methodology. More realistic three-dimensional simulations of a multicell thunderstorm and of trapped lee waves were also analyzed for meteorologically-relevant errors and their sensitivity to one-way and two-way nesting. Nesting was implemented in a similar fashion in both the 1D and 3D models, including the use of either a simple interpolation BC or a sponge layer similar to that used in some modern mesoscale models such as WRF.

The 1D linearized shallow-water equations were used as they are the simplest system supporting waves moving in different directions. Numerical dissipation can effectively remove reflections at a nested boundary in problems like scalar advection, where the only waves that can propagate backwards off the boundary are very poorly resolved. However in many physically significant applications well-resolved signals can propagate in both directions across the grid, and in such cases dissipation cannot be relied on to remove the reflected wave unless that dissipation is strong enough to also remove other physically-important waves.

We compared the relative performance of one-way and two-way nesting in transmitting waves through the nested grid boundary. For moderately-well-resolved shallow-water waves on the coarse grid—which were very well-resolved on the nested grid—two-way nesting was found to yield substantially smaller reflections than did one-way nesting. This result was found to be robust to the choice of BC and the formulation thereof. On a one-way nest, the sponge BC gave the least reflection, but even a very wide 15-point sponge layer still produced much more reflection for these well-resolved solutions.

The two-way nesting strategy keeps the solution on the coarse and nested grids in phase, allowing more consistent coarse-grid fields to be supplied to the nested-grid BC so that well-resolved disturbances are able to exit the nested domain with only minor reflections. These reflections are found to be related to the difference in computational group velocities between the two grids, which increases with decreasing wavelength. In contrast, the solutions on each grid in a one-way nest need not remain in phase and significant differences may develop between the two grids. As a result, the data provided to the boundary conditions from the coarse grid need not match the solution on the one-way nested grid, and nontrivial reflections typically occur. Even small differences in the numerical phase speeds between waves on the coarse and nested grids can gradually accumulate so that when a disturbance reaches the one-way nest's boundary, there is a significant difference between its phase on each grid.

Different behaviors occur if the coarse-grid solution is poorly-resolved. For short-wavelength localized disturbances, the two solutions in a *one-way* simulation may propagate at such different group velocities that the nested-grid solution can reach the nested-grid boundary well before the coarse-grid solution does, so that the coarse-grid solution is zero as the nested grid solution exits. This causes total reflection if the interpolation BC is used, but the sponge BC becomes a wave-absorbing layer which damps the nested-grid solution to zero, increasing its effectiveness compared to when it damps to an out-of-phase solution.

For *two-way* nesting, a marginally-resolved nested-grid solution is transmitted onto the coarse grid as either a shorter wavelength propagating mode or an evanescent mode with zero group velocity. In these cases, the reflection is total when using the interpolation BC, and the reflections for the sponge BC are greatly increased as the presence of an inconsistent coarse-mesh solution in the sponge zone interferes with the absorption of the outgoing waves. This problem may be rectified by spatially filtering the coarse grid data supplied to the sponge, thereby attenuating any short-wavelength coarse-grid disturbances. Adding this filter to the sponge BC modestly decreases the reflections on a one-way nest, and greatly reduces them on a two-way nest.

These results suggest that, two-way nesting is preferred to one-way nesting in the shallow water system given its superiority for well-resolved waves, and that it is no worse than one-way nesting for poorly-resolved solutions if a filter is added to the sponge BC. Unsurprisingly, the sponge and filtered sponge BCs are seen to uniformly produce smaller reflections than does the interpolation BC.

How do these results extend to the more complicated flows? In the multicell simulations, two-way nesting was found to be decidedly superior. When one-way nesting was used, large precipitation errors were produced when the storm attempted to exit the nested grid boundary, regardless of the BC used. Precipitation errors as large as 20% extended into the interior of the nested grid, and were caused even before the storm itself reached the nested grid boundary. Using two-way nesting decreased the error caused by the storm exiting the nested grid and nearly eliminated the errors in the interior.

The storm was found to develop very differently between the two grids. On the coarse grid of a one-way nested simulation where the grid spacing was 3 km, the storm propagated more slowly and developed a weaker updraft and cold pool than did the storm on the nested grid with a grid spacing of only 1 km. Since the nested grid storm reaches the boundary before that on the coarse grid, there was a mismatch at the boundary in the one-way case. From our experience with the 1D shallow water model, we then expect reflections to occur, causing the spurious precipitation near the boundary. Furthermore, the gravity waves generated by the updrafts also formed differently on the two grids, and were also mismatched and reflected. The reflected gravity waves then interfered with the development of the existing storm, or triggered spurious new convective cells, introducing more precipitation errors without the storm itself being near a boundary.

Alternately, two-way nesting has none of the severe problems of one-way nesting. Neither the storm nor the convectively-generated gravity waves have substantial difficulty exiting the nested grid. The minor precipitation errors seen in the two-way simulations are entirely due to the storm propagating onto the coarse grid, and the gravity waves are well-resolved enough to exit the nested grid with only minor reflection.

The simulations of trapped lee waves were more equivocal as to whether one-way or two-way nesting was superior: substantial sensitivity to the nesting methodology, nested grid BC, and accuracy of the numerical method was observed. However, the theory developed with the 1D shallow water model was able to explain much of the behavior of reflected disturbances, and some conclusions about the use of one- and two-way nesting can be drawn.

The trapped wave causes reflections when it attempts to exit the nested grid, producing "primary reflections" propagating inward from the downstream boundary apparent in the vertical velocity field. These reflections are typically larger in two-way nesting. The primary reflection also reflects off the *upstream* boundary, creating a "secondary reflection". In one-way nesting, this reflection occurs because there is a significant mismatch between the coarse-grid solution and the primary reflection, resulting in a secondary reflection that can be larger than the primary reflections. The secondary reflection is typically of lower amplitude in two-way nesting because the well-resolved upstream-propagating mode can easily propagate onto the coarse mesh. The secondary reflection is large enough in one-way nesting when using the interpolation BC that the overall errors were larger than in two-way nesting.

The trapped wave was seen to behave very differently depending on the grid resolution. Unlike the nested grid, which had a well-defined trapped wave in our simulations, the coarse grid would not support a strong trapped wave. In the one-way simulations this would cause reflections again by the mismatch in the solutions at the boundary, but more interesting behavior was seen in the two-way simulations. If the coarse grid does not support a trapped wave, or only allows a trapped wave with a much reduced propagation speed, we expect the reflections to be large due to the change in group velocity between the grids. This sudden, radical change in behavior at the nested grid boundary may explain why the primary reflections are so large in two-way nesting. The changes in wave behavior at the boundary could also create an inconsistent coarse grid solution which interferes with the ability of the BC to damp the outgoing wave (much like the behavior of the 1D shallow water model with marginally-resolved waves), causing larger errors when using the sponge BC instead of the interpolation BC. These claims remain unproven and are a subject for further research. In contrast, reflections in the one-way case are decreased in amplitude by the sponge BC, and errors are overall slightly lower with one-way instead of two-way nesting when the sponge BC is used.

Errors in neither the multicell nor the lee wave simulations were substantially reduced by using the filtered sponge BC. While in the 1D model the filtered sponge worked by removing short-wavelength modes that interfered with the sponge BC, none of the 3D coarse grid solutions were dominated by modes that could be eliminated by our filter and thus the coarse-grid data being relaxed to would be little changed.

In spite of the equivocal results from the trapped wave simulations, the results from the 1D shallow water and 3D multicell simulations suggest that modelers with a choice of nesting methodologies use two-way nesting. Keeping the coarse and nested grids in sync avoids the accumulation of phase errors which can cause large reflections in one-way nesting even for disturbances which are well-resolved on the nested grid. The trapped wave results could imply that two-way nesting gives best results for propagating, localized phenomena, and may be less effective for steady, continually-forced features such as mountain waves.

A drawback of two-way nesting is that it can lead to a cosmetic distortion of the coarse grid solution in the vicinity of the nested grid boundary. Modelers who are using one-way nesting to avoid such distortions should consider switching to two-way nesting and computing a second relatively inexpensive coarse-grid solution without the nested grid that can be used to display the coarse-grid solution without distortion.

BIBLIOGRAPHY

Carpenter, K., 1982: Note on the paper, Radiation conditions for lateral boundaries of limited area numerical models. *QJR Meteorol. Soc*, **110**, 717–719.

Chen, C., 1991: A Nested Grid, Nonhydrostatic, Elastic Model Using a Terrain-following Coordinate Transformation: The Radiative-nesting Boundary Conditions. *Mon. Wea. Rev.*, **119 (12)**, 2852–2869.

Clark, T. and R. Farley, 1984: Severe Downslope Windstorm Calculations in Two and Three Spatial Dimensions Using Anelastic Interactive Grid Nesting: A Possible Mechanism for Gustiness. *J. Atmos. Sci*, **41 (3)**, 329–350.

Colle, B., J. Wolfe, W. Steenburgh, D. Kingsmill, J. Cox, and J. Shafer, 2005: High-Resolution Simulations and Microphysical Validation of an Orographic Precipitation Event over the Wasatch Mountains during IPEX IOP3. *Mon. Wea. Rev.*, **133 (10)**, 2947–2971.

Davies, H., 1976: A lateral boundary formulation for multi-level prediction models. *Quarterly Journal of the Royal Meteorological Society*, **102 (432)**, 405–418.

Deng, X. and R. Stull, 2005: A Mesoscale Analysis Method for Surface Potential Temperature in Mountainous and Coastal Terrain. *Mon. Wea. Rev.*, **133 (2)**, 389–408.

Durran, D., 1991: The third-order Adams-Bashforth method: An attractive alternative to leapfrog time differencing. *Monthly Weather Review*, **119 (3)**, 702–720.

Durran, D., 1999: *Numerical Methods for Wave Equations in Geophysical Fluid Dynamics*. Springer.

Durran, D. R. and J. Klemp, 1983: A compressible model for the simulation of moist mountain waves. *Mon. Wea. Rev.*, **111**, 2341–2361.

Elsberry, R., 1978: Prediction of atmospheric flows on nested grids. *Computational Techniques for Interface Problems*, K. C. Park and D. K. Gartling, Eds., American Society of Mechanical Engineers, No. 30 in Applied Mechanics Division, 67–86.

Fovell, R., D. Durran, and J. Holton, 1992: Numerical Simulations of Convectively Generated Stratospheric Gravity Waves. *Journal of the Atmospheric Sciences*, **49 (16)**, 1427–1442.

Giorgi, F. and L. Mearns, 1999: Regional climate modeling revisited: an introduction to the special issue. *J. Geophys. Res*, **104 (D6)**, 6335–6352.

Harrison, E. and R. Elsberry, 1972: A method for incorporating nested finite grids in the solution of systems of geophysical equations. *Journal of the Atmospheric Sciences*, **29 (7)**, 1235–1245.

Klemp, J. and D. R. Durran, 1983: An upper boundary condition permitting internal gravity wave radiation in numerical mesoscale models. *Mon. Wea. Rev.*, **111**, 430–444.

Klemp, J. and R. Wilhelmson, 1978: The simulation of three-dimensional convective storm dynamics. *Journal of the Atmospheric Sciences*, **35 (6)**, 1070–1096.

Knievel, J., G. Bryan, and J. Hacker, 2007: Explicit numerical diffusion in the WRF Model. *Monthly Weather Review*, **135 (11)**, 3808–3824.

Krol, M., et al., 2005: The two-way nested global chemistry-transport zoom model TM5: algorithm and applications. *Atmos. Chem. Phys*, **5**, 417–432.

Kurihara, Y., G. Tripoli, and M. Bender, 1979: Design of a Movable Nested-Mesh Primitive Equation Model. *Mon. Wea. Rev.*, **107 (3)**, 239–249.

LeVeque, R., 1996: High-resolution conservative algorithms for advection in incompressible flow. *SIAM J. Numer. Anal.*, **33**, 627–665.

Mahalov, A. and M. Moustaoui, 2009: Vertically nested nonhydrostatic model for multiscale resolution of flows in the upper troposphere and lower stratosphere. *Journal of Computational Physics*, **228 (4)**, 1294 – 1311.

Mar-Or, A. and D. Givoli, 2006: The global-regional model interaction problem-analysis of carpenter's scheme and related issues. *Int. J. Multiscale Comput. Eng. v4*, 617–646.

Mass, C., D. Ovens, K. Westrick, and B. Colle, 2002: Does increasing horizontal resolution produce more skillful forecasts? the results of two years of real-time numerical weather prediction over the pacific northwest. *Bull. Amer. Meteor. Soc.*, **83**, 407–430.

Moeng, C., J. Dudhia, J. Klemp, and P. Sullivan, 2007: Examining Two-Way Grid Nesting for Large Eddy Simulation of the PBL Using the WRF Model. *Monthly Weather Review*, **135 (6)**, 2295–2311.

Nance, L. and D. R. Durran, 1997: A modeling study of nonstationary trapped mountain lee waves. Part I: Mean-flow variablility. *J. Atmos. Sci.*, **54**, 2275–2291.

Nance, L. and D. R. Durran, 1998: A modeling study of nonstationary trapped mountain lee waves. Part II: Nonlinearity. *J. Atmos. Sci.*, **55**, 1429–1445.

Peng, X., F. Xiao, and K. Takahashi, 2006: Conservative constraint for a quasi-uniform overset grid on the sphere. *Quarterly Journal of the Royal Meteorological Society*, **132 (616)**, 979–996.

Phillips, N. and J. Shukla, 1973: On the Strategy of Combining Coarse and Fine Grid Meshes in Numerical Weather Prediction. *J. Appl. Meteor.*, **12 (5)**.

Piani, C., D. R. Durran, M. Alexander, and J. Holton, 2000: A numerical study of three-dimensional gravity waves triggered by deep tropical convection and their role in the dynamics of the QBO. *J. Atmos. Sci.*, **57 (22)**, 3689–3702.

Reinecke, P. and D. Durran, 2009: The Overamplification of Gravity Waves in Numerical Solutions to Flow over Topography. *Monthly Weather Review*, **137 (5)**, 1533–1549.

Schroeder, G. and K. Schlünzen, 2009: Numerical dispersion of gravity waves. *Mon. Wea. Rev.*, **137**, 4344–4354.

Skamarock, W. and J. Klemp, 1993: Adaptive grid refinement for two-dimensional and three-dimensional nonhydrostatic atmospheric flow. *Mon. Wea. Rev.*, **121**, 788–804.

Skamarock, W., J. Klemp, J. Dudhia, D. Gill, D. Barker, W. Wang, and J. Powers, 2005: A description of the Advanced Research WRF Version 2. *NCAR Tech Notes-468+ STR*, 88.

Staniforth, A., 1997: Regional modeling: A theoretical discussion. *Meteorol. Atmos. Phys.*, **63**, 15–29.

Sundstrom, A. and T. Elvius, 1979: Computational problems related to limited area modelling. *Numerical Methods Used in Atmospheric Models*, **2**, 379–416.

Vichnevetsky, R., 1981: Propagation through numerical mesh refinement for hyperbolic equations. *Math. Comput. Simulation*, **23**, 344–353.

Warner, T., R. Peterson, and R. Treadon, 1997: A tutorial on lateral boundary conditions as a basic and potentially serious limitation to regional numerical weather prediction. *Bull. Amer. Meteor. Soc.*, **78 (11)**, 2599–2617.

Weisman, M. and J. Klemp, 1982: The Dependence of Numerically Simulated Convective Storms on Vertical Wind Shear and Buoyancy. *Monthly Weather Review*, **110 (6)**, 504–520.

Weisman, M., W. Skamarock, and J. Klemp, 1997: The resolution dependence of explicitly modeled convective systems. *Monthly Weather Review*, **125 (4)**, 527–548.

Zhang, D.-L., H.-R. Chang, N. L. Seaman, T. Warner, and J. Fritsch, 1986: A two-way interactive nesting procedure with variable terrain resolution. *Mon. Wea. Rev.*, **114**, 1330–1339.

VITA

Lucas Harris was born and raised in Rockford, Illinois. He earned a Bachelor's degree in Meteorology and Applied Mathematics from Northern Illinois University in 2003, and after a brief position studying Chicago's lake breeze at Argonne National Laboratory entered the Department of Atmospheric Sciences at the University of Washington. Lucas specializes in mesoscale meteorology and methods for numerical modeling of the atmosphere.